RSC Advances

PAPER

View Article Online
View Journal | View Issue

Cite this: *RSC Adv.*, 2016, **6**, 11461

Removal of cationic and anionic dyes from aqueous solution with magnetite/pectin and magnetite/silica/pectin hybrid nanocomposites: kinetic, isotherm and mechanism analysis†

Olivia A. Attallah,[a] Medhat A. Al-Ghobashy,[bc] Marianne Nebsen*[ab] and Maissa Y. Salem[b]

Novel adsorbents, magnetite nanoparticles modified with pectin shell and silica/pectin double shell, were fabricated and tested for single dye and dye mixture adsorption from water samples. Cationic dyes methylene blue (MB) and crystal violet (CV) and anionic dyes methyl orange (MO) and Eriochrome black T (EBT) were employed to assess dye removal efficiency. The influence of pH, amount of adsorbent, initial dye concentration and contact time was investigated. Results indicated that the optimum pH for removing cationic dyes was 8.0 and 2.0 for anionic dyes. The kinetic studies showed rapid sorption dynamics following a second-order kinetic model. Dye adsorption equilibrium data were fitted well to the Sips isotherm for cationic and anionic dyes. The maximum monolayer capacity, (q_{max}) for MB, CV, EBT and MO was calculated from Sips as 197.18, 180.29, 65.35 and 26.75 mg g^{-1} respectively for magnetite/silica/pectin NPs and 168.72, 140.49, 72.35 and 27.22 mg g^{-1} respectively for magnetite/pectin nanoparticles. For dye mixture adsorption, a new HPLC assay was proposed for quantitation of dyes in treated samples. The results came in accordance with that of single dye adsorption where the magnetite/pectin NPs showed preferred adsorption to anionic dyes while the magnetite/silica/pectin NPs had more affinity to cationic dyes. Thus, our proposed NPs can be used as cheap and efficient adsorbents for removal of cationic and anionic dyes from aqueous solutions.

Received 6th November 2015
Accepted 11th January 2016

DOI: 10.1039/c5ra23452b

www.rsc.org/advances

1. Introduction

Dyes are one of the most hazardous materials in industrial effluents.[1] Common dyes include acidic, basic, reactive, disperse, and direct dyes which usually have an aromatic structure and azo groups.[2] Such structures and their degradation products can cause severe health problems in humans, since they exhibit high toxicity and potential mutagenic and carcinogenic effects.[3,4] The colors in wastewater can also decrease the transparency of water, consume oxygen and elevate biochemical oxygen demand destroying aquatic life.[5,6] Therefore, the removal of dyes from industrial effluents has attracted growing attention in the past decades. Several techniques such as biological treatment, chemical oxidation, membrane separation coagulation/flocculation, adsorption and ion exchange have been developed.[1] Among these methods, adsorption is considered to be simple and highly efficient. A wide range of materials have been reported for dye removal, including, zeolite, clay, activated carbon, polymer, eggshell particles, *etc.*[1,7]

Nonetheless, there are disadvantages associated with such materials. For instance, zeolites adsorption capacity is poor and provides low dye removal efficiency.[8] Activated carbon has some disadvantages since it only transfers the dyes from the liquid phase to the solid phase.[9] Thus, development of new materials with good adsorption capacity, large surface area and small diffusion resistance characteristics is still crucial.[1,5]

Nanotechnology, as a novel method, offers a class of promising adsorbents that are ultra-fine with large surface area and possess magnetic properties to facilitate efficient separation within a short time by applying an external magnetic field.[5] Magnetic nanoparticles have received considerable attention due to the simple procedure involved in synthesis with low capital cost compared to commercially available adsorbents.[10] The magnetic separation is more efficient than other separation methods like filtration or centrifugation and provides online separation of nanoparticles which facilitates the water purification process.[11] Moreover, the magnetic separation has the advantage of recovering the dye and reusing the nanoparticles for multiple cycles of adsorption.

[a]*Pharmaceutical Chemistry Department, Faculty of Pharmacy, Heliopolis University, Egypt*

[b]*Analytical Chemistry Department, Faculty of Pharmacy, Cairo University, Egypt. E-mail: marianne.morcos@pharma.cu.edu.eg*

[c]*Bioanalysis Research Group, Faculty of Pharmacy, Cairo University, Egypt*

† Electronic supplementary information (ESI) available. See DOI: 10.1039/c5ra23452b

Table 1 Chemical structures of the model dyes in the present study[25–28]

Dye	IUPAC name	Structure	Physical characters			
			M_{wt}	log P	pK_a	Solubility (mg L^{-1})
Methyl orange (MO)	Sodium; 4-[[4(dimethylamino)phenyl] diazenyl]benzenesulfonate	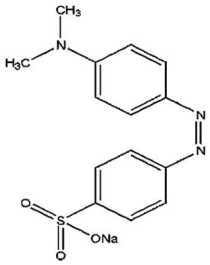	327.33	—	3.4	0.2×10^3
Eriochrome black T (EBT)	Naphthalenesulfonic acid, 3-hydroxy-4-[(1-hydroxy-2-naphthyl)azo]-7-nitro-, sodium salt	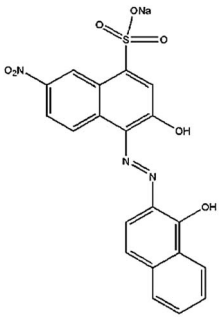	461.37	—	6.2, 11.55	20×10^3
Methylene blue (MB)	[7-(Dimethylamino)phenothiazin-3-ylidene] dimethylazanium; chloride	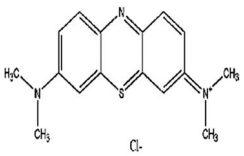	319.85	5.85	3.8	43.6×10^3
Crystal violet (CV)	Tris(4-(dimethylamino)phenyl)methylium chloride	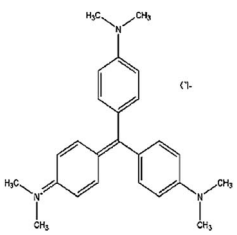	407.21	1.46	5.31, 8.64	4×10^3

The stability of iron oxide nanoparticles, in terms of non-aggregated colloidal dispersion and non-leaching of iron, remains a challenge which could be overcome by surface coating with appropriate coating materials.[12–14] Besides, these coatings can provide functional groups for interaction with various types of compounds. For instance, nano magnetites modified by polyacrylic acid,[15] gum arabic[16] and poly glutamic acid[6] have been used to remove pollutants.

Pectin present within all higher plant cell walls is a structural polysaccharide with partially esterified polygalacturonic acid (PGA).[17] Pectin is considered a valuable byproduct that can be obtained from fruit wastes.[18] Generally, "fruit wastes" is a problem to the processing industries and pollution monitoring agencies. The recovery of by-products like pectin from fruit wastes can improve the overall economics of processing units. Thus, the problem of environmental pollution also can be reduced.[19] Pectin can be extracted from different fruit wastes as nutmeg rind, passion fruit rind, pomelo peel, banana peel and citrus peel.[20] Pectin is also useful as a thickening agent for various food products such as sauces, dairy products, flavored syrups and finds numerous applications in pharmaceutical and cosmetic preparations.[21,22] Besides, pectin, with its numerous functional groups such as carboxyl–carboxylate and hydroxyls, can remove dyes and metal ions.[6] Hybrid nanomaterials of pectin and magnetite nanoparticles have been reported.[23] These nanomaterials combine the biosorbent ability of pectin and magnetic properties of magnetite to remove the pollutants. For example, the adsorption behavior of pectin–iron oxide magnetic adsorbent has been investigated for the removal of methylene blue and Cu metal from aqueous solution.[6]

In the present work the fruit wastes by-product pectin was used as the main agent for adsorption of cationic and anionic dyes. Crystal violet (CV), methylene blue (MB) were used as examples of cationic dyes while Eriochrome black T (EBT) and

methyl orange (MO) as models for anionic dyes (physicochemical properties and 2D structures are summarized in Table 1). We modified the surface of synthesized magnetite nanoparticles (MNPs) by pectin *via* two methods: (1) one step *in situ* synthesis of magnetite–pectin nanoparticles (MP NPs) *via* co-precipitation technique[24] and (2) a two-step fabrication process including modification with a silica shell (magnetite/silica nanoparticles, MS NPs) then adsorption of a pectin shell over the silica shell (magnetite/silica/pectin nanoparticles, MSP NPs). The novel nano-bioadsorbents; MP NPs and MSP NPs, were characterized by transmission electron microscopy (TEM), X-ray diffraction (XRD), Fourier transform infrared (FTIR) spectroscopy, vibration sample magnetometer (VSM) and zeta potential. Such novel nano-adsorbents were compared for their adsorption behavior to reach a high removal efficiency of cationic and anionic dyes from aqueous solutions. The effect of various parameters such as contact time, solution pH, adsorbent mass and initial dye concentration on the adsorption of the model dyes onto the novel bio-adsorbents was systematically studied. Adsorption isotherm, kinetic and mechanism were also evaluated and the obtained results were compared. Simultaneous removal of cationic and anionic dyes from aqueous solutions has also been investigated.

2. Experimental

2.1. Instrumentation

A UV-VIS spectrophotometer model AE-S90-MD form A & E Lab (UK) with 1 cm matched quartz cells was used for determination of dyes concentration. HPLC system model 1100 (Agilent Technologies, USA) with variable wavelength detector and an auto sampler was used for determination of dye mixtures.

2.2. Reagents and materials

Ferric chloride ($FeCl_3$), ferrous sulphate ($FeSO_4 \cdot 7H_2O$), pectin from the rind of citrus or apple (galacturonic acid $\geq$ 74.0%) and tetraethoxysilane (TEOS) were purchased from Fisher Scientific (USA). Methyl orange (CI 13025, CAS 30065-G25, purity 85%) and Eriochrome black T (CI 14645, CAS 260320 G25, purity 85%) were supplied from S D Fine-Chem Ltd. (India). Mehtylene blue (CI 52015, CAS 61-73-4, purity 85%) was supplied from Muby chemicals (India) and crystal violet (CI 42535, CAS 548-62-9, purity 85%) was supplied from Lobachemie (India). HPLC grade acetonitrile and methanol were purchased from Fisher scientific (UK). Ammonium acetate was purchased from Sigma Aldrich (Germany). All other chemicals and reagents used were of analytical grade or higher. Ultra-pure water was obtained using a MilliQ UF-Plus system (Millipore, Eschborn, Germany) with a resistivity of at least 18.2 MΩ cm at 25 °C and TOC value below 5 ppb.

2.3. Analysis techniques

2.3.1. Spectrophotometric method. Standard solutions of each dye (10 mg L^{-1}) were prepared in water (CV, MB, and MO) or in 0.1 N NaOH in the case of EBT. Solutions were scanned in the range of 400–700 nm and the wavelength of maximum absorption for each dye was determined. Accurate volumes of each of CV, MB, EBT, and MO stock solution were transferred into 25 mL volumetric flasks and diluted to volume with the corresponding solvent. Calibration curve for each compound was obtained by plotting absorbance at the λ_{max} of each dye against concentration. Various assay validation parameters were then calculated according to ICH guidelines.[29–31]

2.3.2. Chromatographic method

Optimization and system suitability. HPLC chromatographic separation was achieved using a Thermo electron corporation Betasil C8 column (250 × 4.6 mm, 5 μm). Gradient elution using a mobile phase: (A) acetonitrile and (B) ammonium acetate buffer, pH 6.8 was achieved as follows: 0.0–5.5 min (40% A to 60% B, 1 mL min^{-1}), 5.5–6.0 min (65% A to 35% B, 2 mL min^{-1}), 6.0–7.0 min (85% A to 15% B, 2 mL min^{-1}), 7.0–9.0 min (79% A to 21% B, 2 mL min^{-1}), 9.0–11.0 min (60% A to 40% B, 2 mL min^{-1}) and 11.0–13.0 min (40% A to 60%, 1 mL min^{-1}). Analyses were performed at ambient temperature, detection was carried out at 520 nm and the injection volume was 20 μL.

Calibration and validation. Accurately measured aliquots of working standard solutions equivalent to (50–250 mg L^{-1}) of each dye were separately transferred into a set of 25 mL volumetric flasks and then completed to volume with (1 : 1 methanol : ammonium acetate buffer; pH 6.8). Analysis was carried out as described and the calibration curve for each compound was obtained by plotting area under the peak against concentration. Assay validation was carried out as per ICH guidelines.[29–31]

2.4. Preparation of modified magnetite nanoparticles

2.4.1. Synthesis of core–shell MP NPs *via in situ* co-precipitation. The synthesis of core–shell MP NPs was performed with the modification of the previous literatures.[24,32] The modified method involves the preparation of pectin solutions of different concentrations (0.3, 0.5, 0.7 and 1.0% w/v) by dissolving the corresponding masses in 250 mL distilled water, in a rounded bottom flask. The prepared solutions were then left under continuous stirring for 24 h at room temperature. A 50 mL solution of a 2 : 1 molar ratio of ferric and ferrous ions was added drop wise into the pectin solution under vigorous mechanical stirring. The volume of solution was maintained at 300 mL and stirred for an additional 20 min. The ammonia solution (33 wt%) was then added drop wise till the solution became completely black indicating the formation of magnetite. The mixture was stirred for another 30 min and the black precipitate was collected, washed with distilled water, dried in the oven at 90 °C, and grinded with mortar.

2.4.2. Preparation of double shell MSP NPs

Preparation of MNPs via co-precipitation. The chemical co-precipitation method was employed to synthesize the MNPs. $FeSO_4 \cdot 7H_2O$ and $FeCl_3$ (molar ratio, 1 : 2) were dissolved in 20 mL distilled water and stirred for 20 min. NaOH solution (30 g%) was added drop wise under vigorous stirring until a dark colored precipitate was formed. The solution was then stirred for another 20 min under heating at 70 °C until the dark precipitate turned black. The particles were cooled to room

temperature, magnetically decanted and washed several times with water.

Preparation of core–shell MS NPs. Following Stober process,[33,34] a suspension of the synthesized magnetic nanoparticles (≈1.00 g) was diluted by a mixture of ethanol (80 mL) and water (18.5 mL). After addition of ammonia solution (0.5 mL, 33 wt%), TEOS (1 mL) was added to the reaction solution and mechanically stirred at 25 °C for 16 h. Silica was formed on the surface of magnetite nanoparticles through hydrolysis and condensation of TEOS. The formed MS NPs were then washed three times with deionized water and ethanol using external magnetic decantation.

Preparation of double shell MSP NPs. Pectin solutions of different concentrations (0.3, 0.5, 0.7 and 1% w/v) were prepared by dissolving 0.3 g, 0.5 g, 0.7 g and 1.0 g of pectin in 75 mL distilled water. The prepared solutions were then left under continuous stirring for 24 h at room temperature. Pectin solution was then added drop wise to a 25 mL suspension of the synthesized silica coated magnetic nanoparticles (≈1.00 g) and left stirring for 24 h. The mixture was collected by a permanent magnet, washed with distilled water and dried in the oven at 60 °C for 5 h.

2.5. Single dye adsorption experiments

2.5.1. Experimental design. Preliminary studies were carried out to determine the contact time required to reach equilibrium. Aliquots of 2 g L^{-1} of either MP NPs (0.5 w/v% pectin) or MSP NPs (0.5 w/v% pectin) were added into 50 mL of the dyes solutions of initial concentration (100 mg L^{-1}) at neutral pH and shaken at 25 °C with a speed of 240 rpm. After defined time intervals, samples were removed and the absorbance of dyes left in the supernatant solutions after magnetic separation were determined by using UV-VIS spectrophotometry as described above.

The influence of pH on model dye removal was investigated using 100 mg L^{-1} of dyes solutions over pH range of 2.0–8.0. The pH was adjusted by adding aqueous solutions of 0.1 mol L^{-1} HCl or 0.1 mol L^{-1} NaOH. To each of the pH-adjusted dye solution, 2 g L^{-1} of the adsorbents were added and shaken for 120 min at 25 °C.

To study the effect of adsorbents concentration 0.5, 1.0, 2.0, 3.0, 4.0 and 5.0 g L^{-1} of both adsorbents were added to 50 mL dye solutions (100 mg L^{-1}) with contact time of 120 min. The pH was adjusted at pH 2.0 for anionic dyes and pH 8.0 for cationic dyes. Adsorption capacities were then determined for each adsorbent concentration to determine the optimal concentration of adsorbent that cause complete dye removal.

2.5.2. Calculation of adsorption isotherms. Equilibrium study was conducted by shaking various initial model dye concentrations ranging between 10 and 200 mg L^{-1} separately with 0.5 g L^{-1} of both types of adsorbents (MP NPs and MSP NPs) for 120 min at pH 2.0 for anionic dyes and pH 8.0 for cationic dyes. After equilibrium, the amount of dye adsorbed (q_e, mg g^{-1}) was estimated and plotted against equilibrium concentration (C_e, mg L^{-1}). For plotting equilibrium curves, equilibrium concentration (C_e) was used instead of bulk concentration (C_0) as isotherm models involve C_e and q_e as the *X*- and *Y*-axes coordinates, respectively.

2.5.3. Calculation of kinetics of adsorption. Kinetic study was performed by shaking dye solutions at 10, 50, 100, 150 and 200 mg L^{-1} separately with 0.5 g L^{-1} of both types of adsorbents (MP NPs and MSP NPs) for different time intervals (10–120 min). After each time interval, the concentration of dye in solution was determined and the amount of dye adsorbed at each time interval (q_t, mg g^{-1}) was plotted against time (t, min) for kinetic modeling.

2.6. Desorption experiment

Recovery of model dyes (MB and EBT) from dye-loaded MP NPs and dye-loaded MSP NPs was performed by initially conducting adsorption experiments with a mixture of 100 mg L^{-1} dyes solutions and 2 g L^{-1} of both adsorbents for 120 min. After equilibrium, the dye-loaded NPs were magnetically separated and the supernatant was measured for dye concentration to estimate the amount of dye adsorbed on adsorbent NPs. The dye-loaded NPs were then shaken separately with 50 mL of 5% (v/v) methanol and acetic acid (96%) for 1 h in case of cationic dye (MB) and 50 mL methanol and 50 mL of 5% (v/v) methanol and NaOH in case anionic dye (EBT). The adsorbent was collected by a magnet and reused for adsorption again. The supernatant solutions were analyzed by UV-VIS spectrophotometry to determine the amount of released dye. The cycles of adsorption–desorption processes were successively conducted three times.

2.7. Dye mixture adsorption experiments

Adsorption experiments were carried out in a batch mode by taking 50 mL of the model dyes (MO, EBT, MB and CV) solution mixture containing 165 mg L^{-1} of each dye in 250 mL Erlenmeyer flask. The influence of pH on model dyes removal was investigated over a pH range (2–8) to investigate the efficiency of MP NPs and MSP NPs for selective adsorption of cationic (MB and CV) and anionic (MO and EBT) dyes. The pH was adjusted by adding aqueous solutions of 0.1 mol L^{-1} HCl or 0.1 mol L^{-1} NaOH to the model dyes working solutions. Then to each of the pH-adjusted dyes mixture solutions, 2 g L^{-1} of MP and MSP NPs were added separately and shaken at 25 °C with a speed of 240 rpm. After 2 h samples were removed and the concentration of dyes left in the supernatant solutions after magnetic separation were determined using the HPLC proposed assay. A quantitative determination of dye concentration was achieved by using the linear regression equations, obtained from the calibration curve prepared with a range of dye concentration (50–250 mg L^{-1}).

2.8. Data analyses and modeling

The amount of dye adsorbed at time t, q_t and at equilibrium, q_e, was calculated using the mass balance equation $q_t = (C_0 - C_t)$ (V m^{-1}), where C_0 and C_t (mg L^{-1}) are the initial and final dye concentrations, respectively, V (L) is the volume of the dye solution and m (g) is the mass of adsorbent. When t is equal to the equilibrium time, that is $C_t = C_e$, $q_t = q_e$, then q_e can be

calculated using the same equation as given above. The amount of dyes removed at various solution pH was expressed in percentage (R, %) and calculated using the equation

$$R = 100(C_0 - C_e)/C_0$$

2.9. Statistical analysis

Since error functions are required to assess the kinetic and isotherm models describing the experimental results in a best possible way, the R^2 and chi-square tests are performed to find out the suitability of various kinetic and isotherm models in the present study.[35]

$$\chi^2 = \sum_{i}^{N} \frac{(q_{exp} - q_{cal})^2}{q_{cal}}$$

where, $q_{e,exp}$ and $q_{e,cal}$ (mg g^{-1}) are experimental and calculated dye concentration at equilibrium, respectively and $q_{e,cal}$ (mg g^{-1}) is average value of $q_{e,cal}$.

3. Results and discussion

3.1. Analysis techniques

3.1.1. Spectrophotometric assay. The wavelength of maximum absorption (λ_{max}) was determined for each dye (MB 663 nm, CV 585 nm, MO 465 nm and EBT 531 nm). The method was validated according to ICH Q2B guidelines for validation of analytical procedures as regards in linearity, accuracy, precision (within and between days), limit of detection (LOD), and limit of quantification (LOQ).[29–31] The validation results are summarized in Table 2. In all cases, Beer's law plots were linear with very small intercepts and good correlation coefficients (from 0.9998 to 0.9999). Results indicated the suitability of the assay for accurate determination of the studied dyes. The overlap of the absorption spectra of the four dyes limited the usefulness of this assay for determination of the concentration of the studied dyes when in mixture.

3.1.2. Chromatographic assay. In this experiment, RP-HPLC with gradient elution based on ammonium acetate buffer pH 6.8-acetonitrile was found optimum for the determination of the four dyes in their mixtures. The effect of pH of the mobile phase was studied at acidic pH range; pH 3.5 and 4.5 and poor resolution and peak shape was observed. Flow rate was adjusted at 1 mL min^{-1} to obtain good resolution for MO, EBT and MB then increased to 2 mL min^{-1} to achieve minimum retention times for CV. The VIS detector was operated at 520 nm where appropriate detection sensitivity was achieved.

The retention times were 4.4, 5.1, 5.6 and (7.9, 8.6 and 9.2) min for MO, EBT, MB and CV respectively; as shown in Fig. S1 [a–d].† Good resolution and absence of interference between the dyes being analyzed are shown in Fig. 1.

Peak purity test showed that the peaks having retention times at (7.9, 8.6 and 9.2) min all belong to crystal violet and most probably to its demethylated forms. According to the study of Confortin *et al.* demethylation causes a blue shift in the absorption spectra and a decrease in retention time.[36] Thus it is expected that the peaks at 7.9, 8.6 and 9.2 min are for crystal violet, mono-demethylated crystal violet and di-demethylated crystal violet respectively. In addition, the chromatograms of the dyes in the sample solutions were found identical to the chromatograms received by the standard solutions at the wavelength applied.

System suitability parameters were calculated according to The United States Pharmacopoeia and National Formula and The WHO International Pharmacopoeia,[37,38] and separation efficiency was demonstrated (Table 3). Method validation was carried out according to ICH guidelines.[29–31] Regression equation and validation parameters are summarized in Table 4.

3.2. Characterization of the prepared nanoparticles

3.2.1. TEM. The NPs sizes, pectin and silica coating nature and dispersion of magnetite particle within pectin matrix were examined using Tecani G20, FEI transmission electron microscope (USA). Fig. 2[a] shows the TEM image for pure MNPs which seem to be aggregated due to its dipole–dipole interaction. After coating with silica, the MS NPs had good dispersion due to the repulsion of magnetite particles as shown in Fig. 2[b]. The pure MNPs appear to be almost spherical in shape (ranging from 10 to 20 nm in diameter) and had an overall mean

Table 2 Spectrophotometric method validation for the determination of laboratory prepared standards of model dyes

Item	MO	EBT	MB	CV
Wavelength of detection	465 nm	531 nm	663 nm	585 nm
Range of linearity	1.5–30 μg mL^{-1}	3–30 μg mL^{-1}	0.75–12 μg mL^{-1}	1.5–21 μg mL^{-1}
Regression equation	$A = 0.0723C - 0.0172$	$A = 0.0279C + 0.0024$	$A = 0.1754C + 0.0575$	$A = 0.1053C + 0.0122$
Regression coefficient (r^2)	0.9999	0.9999	0.9999	0.9998
LOD (μg mL^{-1})	0.22	0.55	0.12	0.21
LOQ (μg mL^{-1})	0.65	1.67	0.36	0.63
SD of slope-S_b	0.0004	0.0002	0.0008	0.0008
SD of intercept-S_a	0.008	0.003	0.005	0.01
Accuracy mean ± SD	99.76 ± 0.56	99.59 ± 0.87	100.71 ± 0.79	100.14 ± 0.94
Repeatability (% RSD, $n = 6$)	0.51	1.28	0.44	0.77
Precision				
Intraday % RSD ($n = 3$)	0.17–0.23	0.09–0.1	0.07–1.03	0.03–0.59
Interday % RSD ($n = 3$)	0.14–1.01	0.64–1.44	0.59–1.02	0.43–1.2

diameter of 15 ± 4 nm. After silica coating onto the MNPs, particles had an overall mean diameter of 20 ± 4 nm indicating the formation of silica shell of around 2 nm thickness over the MNPs. Fig. 2[c] illustrates the binding of the 0.5 w/v% pectin onto MS NPs, the particles had an overall mean diameter of 25 ± 5 nm. This indicates that the surface of particles somehow changed after coating with pectin due to formation of double shell layer over MNPs with a total shell thickness of 5 nm. However, the pectin matrix seems to have trapped more than one magnetic core in MSP NPs (1 w/v%) as shown in Fig. 2[d]. Such observation suggests that increasing the concentration of pectin above 0.5 w/v% may cause re-aggregation of particles within the pectin matrix.

TEM analysis of the MP NPs demonstrates that the presence of pectin during the formation of MNPs increases the size of magnetite nanoparticles. However, to a great extent pectin prevented particle aggregation due to the dispersion of magnetite within pectin matrix. Fig. 2[e] shows the MP (0.5 w/v%) nanoparticles with a diameter range of 200–500 nm. On the other hand, Fig. 2[f] illustrates the MP NPs (1 w/v%) ranging from 50 to 100 nm in diameter. Such difference in size of the coated samples indicates that the coating material has an effect on the size of particles which comes in agreement with what was mentioned in previous studies.[39] Having a close look at Fig. 2[e] and [f], the light atoms of carbon, hydrogen and oxygen, which constitute the polysaccharide structure of pectin, correspond to brightest areas. The heavy Fe atom allows a better contrast and corresponds to darkest areas which are scattered as dots within the pectin matrix. In addition, these TEM images show some level of aggregation and non-uniform coating of the MNPs. Nevertheless, there is some improvement in the dispersion of iron oxide particles in pectin matrix than the pure magnetite nanoparticles. Thus it can be concluded that both types of nanoparticles enhanced the dispersion of the MNPs yet the control of particles size in case of MSP NPs was better than that of MP NPs.

3.2.2. XRD. XRD measurements were performed in a Rigaku model Geigerflex apparatus using Cukα radiation from 10 to 70° (2θ) at a scan rate of 4° min^{-1} and silicon as an external standard. The MNPs, synthesized by co-precipitation of Fe^{2+} and Fe^{3+} ions, were confirmed from XRD measurements with diffraction peaks at (2 2 0), (3 1 1), (4 0 0), (4 2 2), (5 1 1), and (4 4 0) by comparison with Joint Committee on Powder Diffraction Standards (JCPDS card, file No. 00-019-0629), which are indexed to the cubic spinel phase of magnetite. As shown in Fig. 3, S2 and S3,† XRD peaks corresponding to these planes were also recorded for MP NPs and MSP NPs. Thus, these results indicate that the modification of magnetite nanoparticles by pectin and silica have not changed the crystal structure of nanoparticles. Nevertheless, in the XRD pattern of MP NPs (1 w/v%) (Fig. S2†), extra peaks were observed which suggests the presence of another form of iron oxide (preferably goethite (JCPDS card, file No. 04-015-8202)) as a result of using pectin in increased concentrations. The silica coating was also confirmed by the presence of diffraction peaks at (0 1 1) which is characteristic for silicon oxide (JCPDS card, file No. 01-075-3165).

The intensity of the peaks corresponding to the surface functional groups was found to be reduced upon using pectin and silica. This reduction for MSP NPs is more than that of MP NPs due to the double shell property of the former. The crystal sizes of the hybrid NPs were also determined from the XRD pattern by using Scherrer's equation;[6]

$$D = \frac{k\lambda}{\beta \cos \theta}$$

where D is the average crystalline diameter, k is Scherrer constant (0.89), λ the X-ray wavelength (0.15405 nm), β the peak width of half-maximum, and θ is the Bragg diffraction angle.

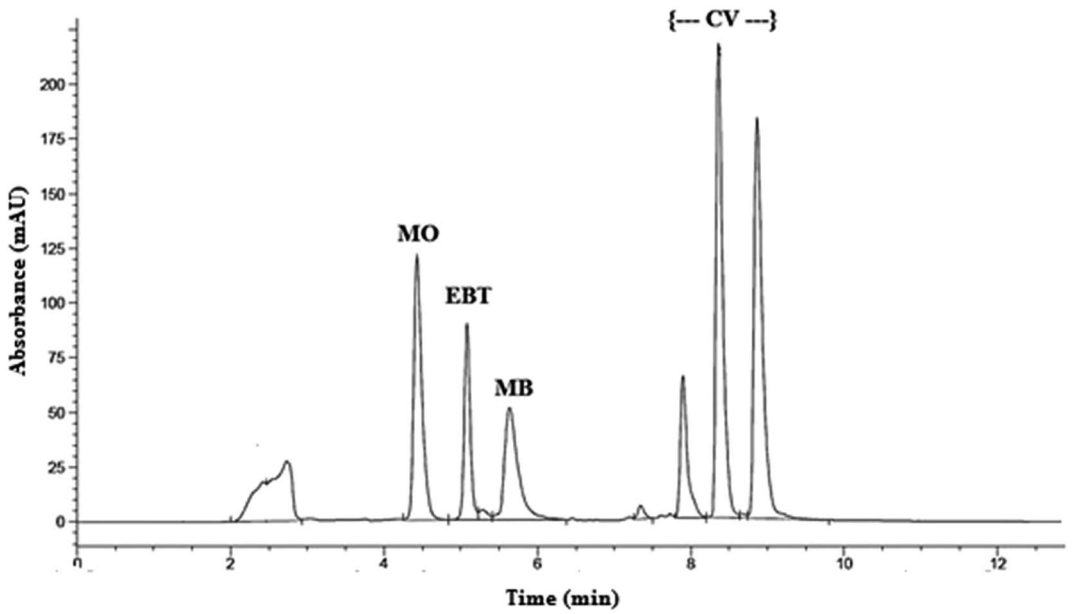

Fig. 1 HPLC chromatogram of model dyes: methyl orange (MO), Eriochrome black T (EBT), methylene blue (MB) and crystal violet (CV).

Table 3 System suitability tests for HPLC method for the simultaneous determination of model dyes (MO, EBT, MB and CV) in their ternary mixture

	Obtained value				
Parameters	MO	EBT	MB	CV	Reference value[37,38]
Retention time (t_R)	4.43	5.08	5.64	7.90	
Symmetry factor (A_s)	1	1.1	1.5	1.5	$T \leq 2$
Theoretical plates number (N)	9151	22 062	5650	46 640	$N \geq 2000$
Capacity factor (k)	1	1.3	1.6	2.6	1–10 acceptable
Resolution (R_s)	2.38	1.51	5.97	—	$R_s \geq 1.5$
Selectivity factor (α)	1.29	1.20	1.66	—	$\alpha > 1$

The average crystal sizes were found to decrease with increase in silica and pectin concentrations. It can also be observed that the average crystal size of the MP NPs (8 nm for MP (0.5 w/v%) and 5 nm for MP (1 w/v%)) is slightly larger than the MSP NPs; 5.5 nm for MP (0.5 w/v%) and 4.6 nm for MP (1 w/v%). This can be attributed to the presence of silica shell which prevented the aggregation of particles causing additional decrease in crystal size as supported by the difference in crystal size of MS NPs (6 nm) and pure MNPs (10 nm). Such results come in agreement with those found in the TEM images.

3.2.3. FTIR. Infrared spectra were collected to investigate if pectin and silica were bound to magnetite nanoparticles. Samples were compacted with KBr (approximately 1%) and analyzed in transmission mode in a Perkin Elmer Spectrum GX spectrophotometer. In the FTIR spectrum of the pure pectin sample (Fig. 4[a]), the peaks at 3445 cm^{-1} and 2932 cm^{-1} represent secondary hydroxyl groups and carboxylic hydroxyl groups, respectively. Also, the peak at 1751 cm^{-1} is a characteristic peak of pectin (representing the carbonyl of the esterified pendant group). The intense peak at 1014 cm^{-1} arises from the glycosidic bonds linking two galacturonic sugar units.[32] Comparing Fig. 4[b] for pure MNPs to Fig. 4[d] for MP NPs (0.5, w/v% pectin) and Fig. S4† for MP NPs (0.3, 0.7 and 1 w/v% pectin) many additional peaks were observed after pectin binding to MNPs, whereas few peaks appeared in MNPs without pectin coating, thus elucidating the successful binding of pectin on MNPs. The appearance of broad peaks at 3374–3431 cm^{-1} was attributed to the O–H stretching vibrations[40] and the peaks at 564–611 cm^{-1} in both MNPs and MP NPs were resulted from the stretching vibration of Fe–O–Fe in magnetite.[41] For MP NPs alone, the peak at 1732–1739 cm^{-1} was assigned to the C–O stretches in free carboxylic acid.[42] The peaks 1401–1403 cm^{-1} is caused by asymmetric and symmetric stretching vibrations of carboxylic acids in ionic form (COO−),[32] and the peak at 1093–1100 cm^{-1} indicated the stretching vibration of C–OH of alcoholic groups and carboxylic acids. The bands at 1016–1022 cm^{-1} are due to the vibrations associated with the skeletal rings of the sugar monomers of pectin.[32] Thus, such findings confirm that pectin strongly binds both iron(III) and iron(II) ions through a COO^- linkage.[24]

The characteristic vibration bands of SiO_2 as listed in literature are mainly: ν_{as}(Si–O–Si) at 1200 cm^{-1} and 1075 cm^{-1}; ν_{as}(Si–OH) at 970 cm^{-1}; ν_s(Si–O–Si) at 795 cm^{-1}; ν(Si–O–Si) from cyclic tetramers at 540 cm^{-1} and δ(Si–O–Si) at 460 cm^{-1}.[43] Noticeably, in Fig. 4[c] representing MS NPs, the absorption of SiO_2 was confirmed by the shift of the ν_{as}(Si–OH) peak at 1037 cm^{-1} and Si–O–Si bond shift at 889 cm^{-1} indicating that iron ions might be bonded to silicate skeleton through O–Si–O–Fe–O–Si–O linkage.[34,43,44] (Si–OH) and Si–O–Si peaks also appeared in the MSP NPs in the range 1044–1055 cm^{-1} and 867–889 cm^{-1} respectively. Such findings illustrate the specific interactions between MNPs and silica which can be covalent, through Si–O–Fe bond formation; electrostatic, between negatively charged Si–O terminal ligands and positively charged

Table 4 HPLC Method validation for the determination of laboratory prepared standards of model dyes

Item	MO	EBT	MB	CV
Retention time	7.90	5.64	5.08	4.43
Wavelength of detection	520 nm	520 nm	520 nm	520 nm
Range of linearity	50–250 μg mL^{-1}	50–250 μg mL^{-1}	50–250 μg mL^{-1}	50–250 μg mL^{-1}
Regression equation	$A = 14.239C + 8.3887$	$A = 18.502C + 8.6695$	$A = 11.702C + 23.923$	$A = 39.749C + 65.485$
Regression coefficient (r^2)	0.9997	0.9997	0.9995	1
LOD (μg mL^{-1})	2.47	1.70	2.80	3.22
LOQ (μg mL^{-1})	7.47	5.14	8.47	9.76
SD of slope-S_b	0.114	0.163	0.129	0.106
SD of intercept-S_a	18.960	27.545	21.517	17.636
Accuracy mean ± SD	99.62 ± 1.03	100.72 ± 1.16	101.04 ± 0.69	101.12 ± 0.89
Repeatability (% RSD, $n = 6$)	0.75	0.51	1.2	1.38
Precision				
Intraday % RSD ($n = 3$)	0.07–0.16	0.22–1.43	0.99–1.34	0.3–1.02
Interday % RSD ($n = 3$)	1.08–1.53	0.4–1.98	0.82–1.34	0.65–1.55

groups on the particle surface; or hydrogen-bond interactions between hydration layers of silanol groups and the particle surface.[45]

Furthermore, there was a disappearance of the peaks 1014 and 1095 cm^{-1} from the MSP NPs spectra (Fig. 4[e] for 0.5 w/v% pectin, and Fig. S5† for 0.3, 0.7 and 1 w/v% pectin) which correspond to the vibrations associated with the skeletal rings of the sugar monomers of pectin and C–OH of alcoholic groups respectively.[32] Such finding can be attributed to the overlapping of OH groups of sugar monomers with the Si–O band of the silica stabilization.[32,44] The appearance of peaks at 1737–1739 cm^{-1} and 1402–1408 cm^{-1} assigned to the stretching vibrations of C–O and carboxylic acids in ionic form (COO^-) respectively, indicates the successful binding of pectin onto the MS NPs.[32,42]

3.2.4. Magnetic properties. The magnetic properties were measured using Princeton EG and G Applied Research VSM, Model 155. The magnetic behavior of the MP NPs 0.5 w/v% (Fig. 5[c] and S6† for 0.3, 0.7 and 1 w/v% pectin) and MSP NPs 0.5 w/v% pectin (Fig. 5[d] and S7† for 0.3, 0.7 and 1 w/v% pectin) was studied by recording magnetization (M) against applied magnetic field (G) at room temperature using VSM. The M–G curve of the coated NPs exhibited negligible coercivity and remanence magnetization and was similar to that of the as-synthesized Fe_3O_4 nanoparticles. This phenomenon was typically due to superparamagnetism, attributed to magnetite nanoparticles.[46] The saturation magnetization (M_s) was found to be 38.7 emu g^{-1} for magnetite and reached 24.4 emu g^{-1} for MSP NPs (1 w/v%) and 5.03 emu g^{-1} for MP (1 w/v%) NPs.

Notably, the saturation magnetization measured in most of our coated NPs was acceptable for potential magnetic separation because M_s of 16.3 emu g^{-1} was sufficient for magnetic separation with a conventional permanent magnet.[47] Compared with MNPs, the saturation magnetization decreased in both types of coated NPs which could be due to the formation of magnetic dead layer by non-magnetic material (pectin) at the domain boundary wall of Fe_3O_4 NPs.[48] Nevertheless, MSP NPs (0.3 w/v% and 0.5 w/v%) showed a greater decrease in saturation magnetization than MP NPs (0.3 w/v% and 0.5 w/v%). Such decrease could be related to the formation of an additional non-magnetic layer of silica in MSP NPs.

It is also worth mentioning that the saturation magnetization of coated samples decreased with increasing pectin concentration. Such result can be attributed to the decrease in

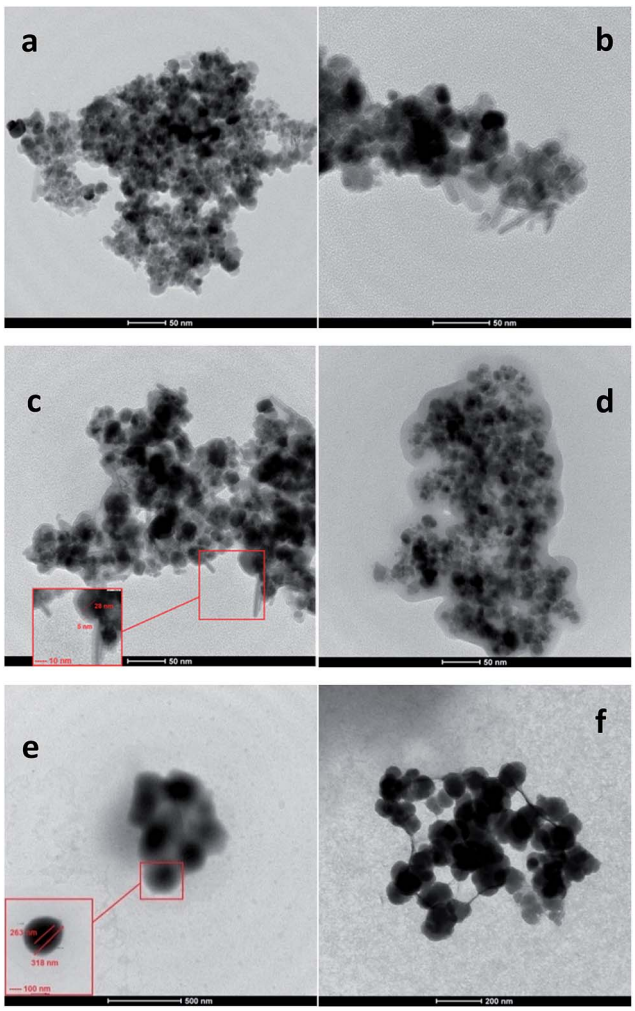

Fig. 2 TEM image of; [a] MNPs, [b] MS NPs, [c] MSP NPs (0.5 w/v%), [d] MSP NPs (1 w/v%), [e] MP NPs (0.5 w/v%), [f] MP NPs (1 w/v%). Magnetite Nanoparticles: MNPs; Magnetite/Silica Nanoparticles: MS NPs; Magnetite/Pectin Nanoparticles: MP NPs and Magnetite/Silica/Pectin Nanoparticles: MSP NPs.

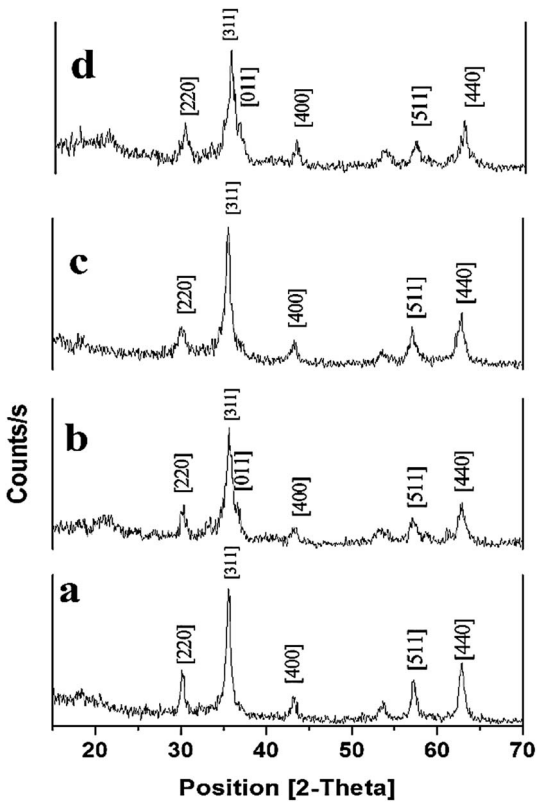

Fig. 3 XRD pattern of; [a] MNPs, [b] MS NPs, [c] MP (0.5 w/v%) NPs, and [d] MSP (0.5 w/v%) NPs. Magnetite Nanoparticles: MNPs; Magnetite/Silica Nanoparticles: MS NPs; Magnetite/Pectin Nanoparticles: MP NPs and Magnetite/Silica/Pectin Nanoparticles: MSP NPs.

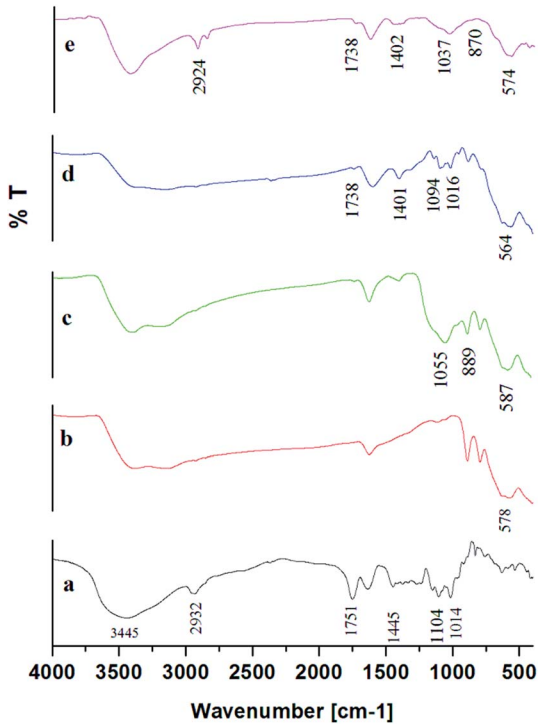

Fig. 4 FTIR data for; [a] pure pectin, [b] MNPs, [c] MS NPs, [d] MP (0.5 w/v%) NPs pectin, and [e] MSP (0.5 w/v%) NPs. Magnetite Nanoparticles: MNPs; Magnetite/Silica Nanoparticles: MS NPs; Magnetite/Pectin Nanoparticles: MP NPs and Magnetite/Silica/Pectin Nanoparticles: MSP NPs.

the amount of MNPs for the same volume of measured samples and thus affect their total magnetic moment. However, despite the increase in pectin concentration the MSP was able to maintain a favorable range of M_s values than the MP NPs. A significant decrease in the M_s of MP NPs (0.7 w/v% and 1 w/v%) reaching 12 and 5 emu g^{-1} respectively was observed and could be due to the formation of goethite phase in the NPs which has decreased M_s than that of magnetite.[18]

3.2.5. Zeta potential. It is well known that the surface charge is one of the dominant factors in deciding the overall adsorption capacity of any adsorbent.[49,50] Surface charge of samples was studied using a Zetasizer Nano ZS, from Malvern Instruments (UK) at neutral pH. Magnetite being an amphoteric solid, can develop positive and negative charges respectively, due to protonation as ($FeOH + H^+ \rightarrow FeOH^{2+}$) and deprotonation ($FeOH + H^+ \rightarrow FeO^- + H^+$) of FeOH sites generated on surface of magnetite when dispersed in water.[51] Hence it is important to determine the point of zero charge (pHzpc) of the modified MNPs so that nature of charge on their surface can be predicted at a given pH. As shown in Fig. 6 the surface charge of magnetite prepared in the absence of the coating agent was negative (−15.1 mV) which implies the presence of hydroxyl ions at the surface of the Fe_3O_4 particles. MP NPs of 0.5 and 1 w/v% also had negative values (−18 and −19.1 mV) respectively which come in agreement with the FT-IR analysis revealing the COO–Fe linkage. The difference in potential values of 0.5 w/v% and 1 w/v% MP NPs samples can be attributed to the variation in pectin concentration. Thus, the polymer coat concentration can have an effect on surface properties of these hybrid particles which comes in accord with literature.[52] The higher negative potential value for the 1 w/v% pectin sample indicates more complete coating of iron surface cations through O–Fe linkage.[24] Similar results were observed with MSP NPs as the 1 w/v% pectin shell showed higher potential value (−26.2 mV) than the 0.5 w/v% shell (−22.1 mV). Noticeably, the variation in the zeta potential values affects the stability of the nanosuspensions. As a rule of thumb, suspensions with zeta potential above 30 mV (absolute value) are physically stable. Suspensions with a potential above 60 mV show excellent stability. Suspensions below 20 mV are of limited stability, below 5 mV they undergo pronounced aggregation.[53] Thus our MSP NPs show better stability in suspensions at neutral pH than MP NPs.

The pHzpc of MP NPs and MSP NPs is found to be 2.2 and 2.5 respectively as illustrated in Fig. 6[b], which compares well with those reported previously for magnetite NPs coated with pectin.[32] Thus, the surface both types of adsorbents will be either positively or negatively charged at pH < 2.5 or pH > 2.5, respectively, which entails the advantage of removal of anionic or cationic dyes from water *via* adsorption at different pH levels.

3.3. Single dye adsorption experiments

3.3.1. Effect of contact time. The effect of contact time on the adsorption of model dyes; CV as an example of cationic dyes and EBT as an example of anionic dyes was studied to determine the time taken by 2 g L^{-1} MSP and MP NPs to remove the studied dyes (100 mg L^{-1}) from solutions at natural pH. The adsorption capacity results of MSP NPs and MP NPs are shown in Fig. 7[a] and [b] respectively. Within the first 60 min there was a significant increase in the adsorption capacity of NPs. Further increase in the contact time was accompanied by slow increase

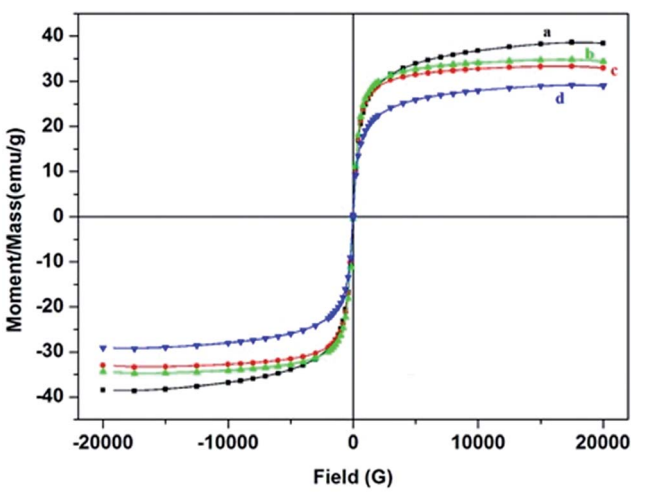

Fig. 5 Hysteresis loop of NPs of; [a] MNPs, [b] MS NPs, [c] MP NPs (0.5 w/v%) pectin, and [d] MSP NPs (0.5 w/v%) pectin. Magnetite Nanoparticles: MNPs; Magnetite/Silica Nanoparticles: MS NPs; Magnetite/Pectin Nanoparticles: MP NPs and Magnetite/Silica/Pectin Nanoparticles: MSP NPs.

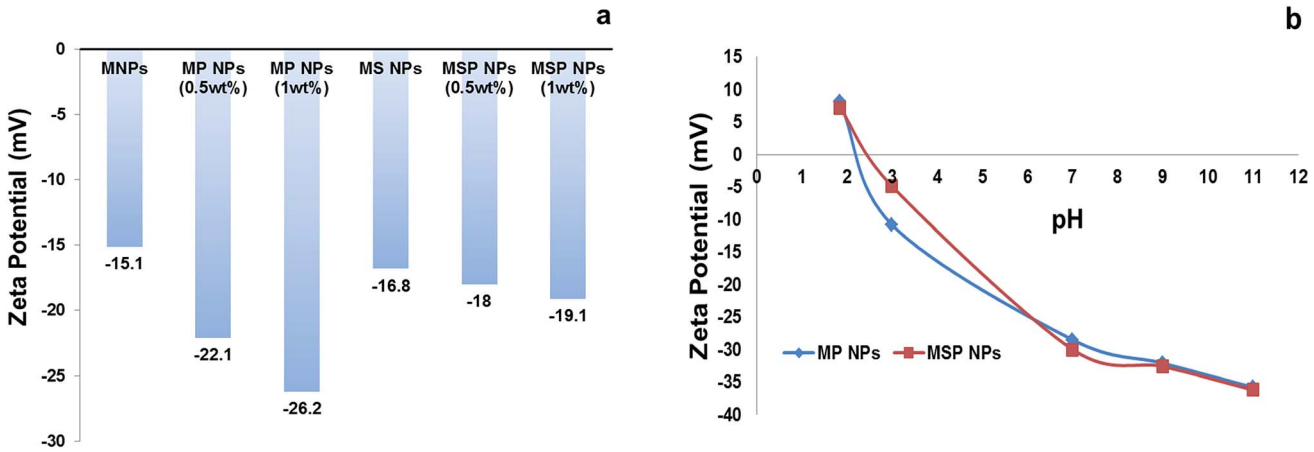

Fig. 6 Zeta potential of the nanoparticles; [a] at neutral pH and [b] at different pH.

in the adsorption capacity of NPs. The MSP NPs showed an adsorption capacity of 33.6 mg g^{-1} for CV and 12 mg g^{-1} for EBT, on the other hand the MP NPs had an adsorption capacity of 30.7 mg g^{-1} for CV and 16.2 mg g^{-1} for EBT after 120 min. The experiment time was extended to 150 min and it was observed that the adsorption of dyes on the NPs reached equilibrium after 120 min. This may indicate that the adsorption starts very fast on the external surface followed by a slower adsorption on the internal surface of the nano-composites. Agitation time of 120 min was selected for further works.

3.3.2. Effect of pH. The effect of pH in the range 2–8 on the removal of the model dyes (MB, CV, EBT and MO) was investigated with initial dye concentration of 100 mg L^{-1} each and 2 g L^{-1} adsorbents mass. As Fig. 8[a] and [b] show, for the cationic dyes (MB and CV) the adsorption was remarkably decreased in pH 2.0. Low pH values (pH < 3.0) were unfavorable for dye adsorption by MP NPs and MSP NPs because of the presence of an excess of H^+ ions that compete with dye cations for the adsorption sites (COO^- and OH) groups. The capacity of dye adsorption for MB and CV increases with increasing the solution pH from 2 to 8, reaching its maximum at 8. The increase in the amount of adsorbed dye when increasing the pH value suggests that the electrostatic interactions between the –COO– and OH present in pectin and the positively charged cationic dyes contribute to the adsorption process.[54]

For the anionic dyes (MO and EBT), as observed in Fig. 8[a] and [b], the adsorption is high in acidic medium and decreases with the increase in solution pH. This can be attributed to the fact that as the pH is lowered, the hydroxyl and carboxylic groups of pectin are protonated and the overall surface charge on the NPs will become positive. Such result will promote reaction with EBT and MO as anionic dyes through electrostatic forces of attraction.

3.3.3. Effect of adsorbent mass. The effect of the adsorbent mass usually determines the solid adsorbent's capacity for a given initial concentration of adsorbate in a solution. Fig. 9[a] and [b] show the effect of the MSP and MP NPs mass on the adsorption of the model dyes from the aqueous solutions respectively. It is clear from the figures that the % of model dyes removed increased gradually as the nanoparticles mass increased. The removal of cationic dyes; MB and CV reached 82 and 75% respectively when 2 g L^{-1} of MSP NPs was employed. On the other hand, the MP NPs showed removal efficiency of 55% and 73% for MB and CV respectively. The anionic dyes % removal declared that 2 g L^{-1} of MSP NPs has removal efficiency of 44% for EBT dye and 8% for MO dye, while removal % of 47%

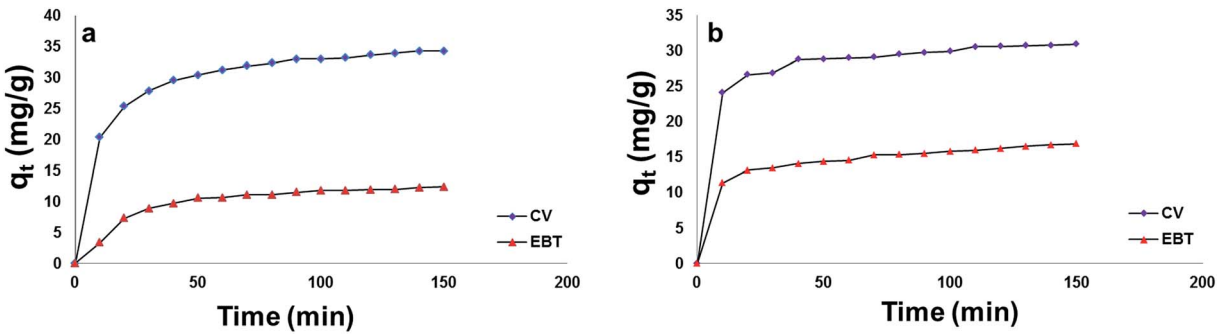

Fig. 7 Effect of contact time on the adsorption capacity (q_t) of EBT and CV onto; [a] MSP NPs and [b] MP NPs. Adsorbent: 2 g L^{-1}, dyes 100 mg L^{-1}, temperature: 25 °C, pH: natural pH of dye, time: 150 min. Magnetite/Pectin Nanoparticles: MP NPs and Magnetite/Silica/Pectin Nanoparticles: MSP NPs.

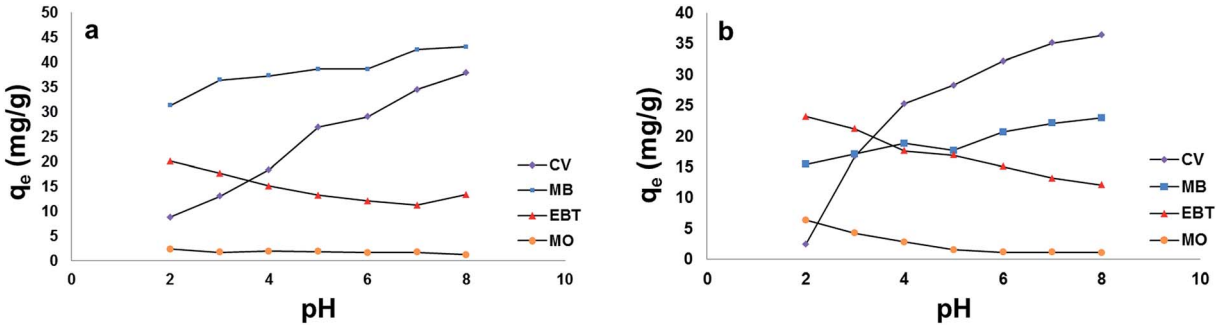

Fig. 8 Effect of pH on the adsorption capacity (q_e) of model dyes onto; [a] MSP NPs and [b] MP NPs. Adsorbent: 2 g L^{-1}, dyes 100 mg L^{-1}, temperature: 25 °C, time: 120 min. Magnetite/Pectin Nanoparticles: MP NPs and Magnetite/Silica/Pectin Nanoparticles: MSP NPs.

and 12.5% for EBT and MO respectively were achieved by MP NPs. The enhancement that was observed in the % removed of model dyes was principally due to the increase in the active sites on the nanoparticles available for adsorption of dyes molecules. Further increase in the dosage of both types of nanoparticles from 3 to 5 g L^{-1} was accompanied by further increase in the % dyes removed to over 90% except for MO. However, the removal of dyes was not linearly increased presumably and this can be attributed to the aggregation of NPs upon increasing their mass from 3 to 5 g L^{-1} which in turn reduced the active sites for adsorption.[55]

3.3.4. Mechanism of the adsorption. The surfaces of MP and MSP NPs are generally covered with hydroxyl and carboxylic groups that vary in forms at different pH. The surface charge is neutral at pHzpc (the pH of zero point charge, pHzpc, of MP nanoparticles is around 2.5). Below the pHzpc, the adsorbent surface is positively charged, and anion adsorption occurs. Such phenomenon was observed with the anionic dyes – EBT and MO. As the pH of the solution increased, a proportional decrease in adsorption took place due to the successive deprotonation of hydroxyl and carboxyl groups on the adsorbent and electrostatic repulsion between negatively charged sites on the adsorbent and dye anions. There was also competition between OH^- (at high pH) and dyes anions for positively charged adsorption sites.[56] Also, the molecular size and the number of anions groups (SO_3^{2-}) on the dye molecule are important factors in their different adsorptive behavior.[57] For instance, EBT showed greater adsorption than MO due to the larger molecular size of EBT in addition to the presence of two sulphonate groups in EBT while there is only one in MO giving EBT a more electronegative surface than MO thus more favorable adsorption on the surface of positively charged NPs.

On the other hand, an increase in cationic dyes – CV and MB – adsorption took place at pHs above the pHzpc of both types of NPs due to the electrostatic attraction between negatively charged sites on the adsorbents and dyes cations. The ionic nature of the two basic dyes (methylene blue and crystal violet) could have played a role in retaining the dye species on the surface of the adsorbents. The molecular structure of methylene blue has ionic charge, with decentralised or delocalised positive charge on its organic structure. Similar arguments could be applied to the structure of crystal violet.[57]

A superior adsorption of cationic dyes on MSP NPs was observed than that on MP NPs while it was the opposite for anionic dyes adsorption. This can be attributed to the presence of an additional silica shell in MSP NPs which offers more negative charge on the surface than MP NPs at elevated pHs. Such condition favors the electrostatic attraction between the negatively charged silanol groups (Si–O) on NPs surface and the positively charged cationic dyes monomers to form a strong hydrogen bond and increasing their adsorption capacity.[58] In addition, MB showed higher adsorption capacity than that of

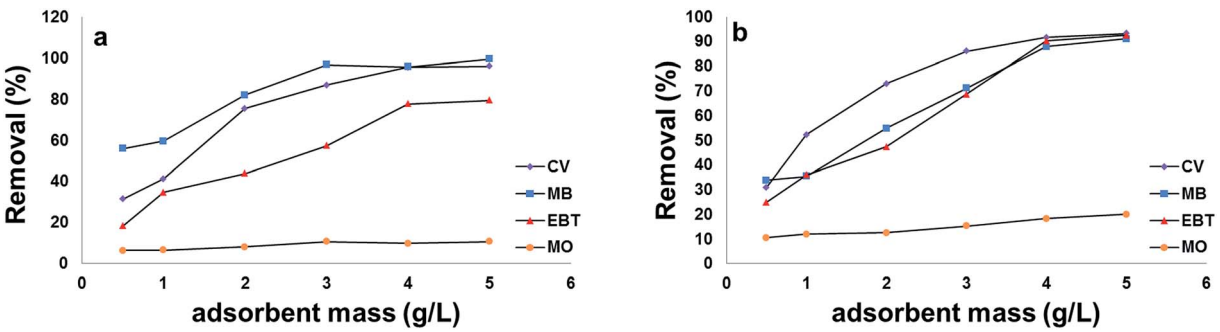

Fig. 9 Effect of adsorbent mass on the removal efficiency of model dyes onto: [a] MSP NPs and [b] MP NPs. Dyes 100 mg L^{-1}, temperature: 25 °C, pH: 2.0 for anionic dyes and 8.0 for cationic dyes, time: 120 min. Magnetite/Pectin Nanoparticles: MP NPs and Magnetite/Silica/Pectin Nanoparticles: MSP NPs.

Table 5 Parameters of adsorption isotherms using Langmuir, Freundlich, Redlich–Peterson and Sips equations for MSP and MP NPs

	Langmuir					Freundlich				Redlich-Peterson					Sips				
	Q_0 (mg g^{-1})	B (mL mg^{-1})	R_L	R^2	χ^2	K_f (mL g^{-1})	$1/n$	R^2	χ^2	$K_{RP} \times 10^3$ (mL g^{-1})	α_{rp} (mL mg^{-1})	β	R^2	χ^2	Q_m (mg g^{-1})	K_s (mL mg^{-1})	$1/n$	R^2	χ^2
MSP NPs																			
CV	125	16	0.2336	0.9922	0.505	328.09	0.648	0.9908	1.854	2	12.8	0.8648	0.9965	0.4235	180.295	1.949	0.6547	0.9987	0.145
MB	185.18	27	0.1583	0.9974	3.888	650.018	1.625	0.9657	7.342	10	46	0.9142	0.9984	0.2817	197.18	2.512	0.5578	0.9971	0.365
EBT	108.69	10.22	0.3318	0.8132	0.816	219.79	0.6268	0.9922	0.231	2.5	12.25	0.5281	0.9232	1.7076	65.35	3.849	0.6688	0.9929	0.655
MO	60.61	3.75	0.5727	0.7382	0.638	102.74	0.8136	0.992	0.470	1.11	11.66	0.1614	0.8252	0.4702	26.754	3.277	0.7277	0.992	0.4704
MP NPs																			
CV	100	25	0.1632	0.9965	0.881	265.52	0.5923	0.9795	3.252	2.5	18.5	0.8196	0.9935	0.8168	140.49	2.085	0.425	0.9973	0.2139
MB	92.59	36	0.1173	0.9929	1.468	210.44	0.4746	0.9797	2.686	10	70	0.7241	0.993	1.357	168.72	1.036	0.6021	0.9897	0.599
EBT	133.33	10.71	0.3149	0.883	2.947	297.56	0.6567	0.9954	0.726	2	8.8	0.6353	0.9485	1.4	72.348	3.212	0.579	0.9925	0.839
MO	126.58	2.82	0.6392	0.6091	1.085	183.48	0.8415	0.9947	0.576	0.37	2.296	0.8061	0.6645	0.9687	27.215	4.3837	0.708	0.9945	0.445

CV on MSP NPs and this might be due to the affinity of MB to the silica shell of MP NPs than that of CV. On the other hand, since the MP NPs offers a lesser negatively charged surface than MSP NPs in acidic pH, it favors the adsorption of anionic dyes than that of MSP NPs.

3.3.5. Adsorption isotherms. The equilibrium adsorption isotherm model, which is the number of mg adsorbed per gram of adsorbent (q_e) *vs.* the equilibrium concentration of adsorbate, is fundamental in describing the interactive behavior between adsorbate and adsorbent.[10] Equilibrium isotherm studies were carried out with different initial concentrations of model dyes (10–200 mg L^{-1}) at 25 °C and pH 2.0 for anionic dyes and pH 8.0 for cationic dyes. Four models were used to analyze the equilibrium adsorption data: Langmuir,[59] Freunlich,[60] Redlich–Peterson[61] and Sips.[62] Langmuir's model does not take into account the variation in adsorption energy, but it is the simplest description of the adsorption process. It is based on the physical hypothesis that the maximum adsorption capacity consists of a monolayer adsorption, that there are no interactions between adsorbed molecules, and that the adsorption energy is distributed homogeneously over the entire coverage surface.[59,60] The general form of the Langmuir isotherm was determined as shown in eqn (1).

$$q_e = \frac{Q_0\, bC_e}{(1 + bC_e)} \quad (1)$$

where C_e is the equilibrium concentration of the dye in the solution (mg mL^{-1}), q_e is the amount of dye adsorbed per unit mass of adsorbent (mg g^{-1}), at equilibrium concentration, C_e, b the Langmuir equilibrium constant (mL mg^{-1}) and related to energy of adsorption. Q_0 signifies the maximum adsorption capacity (mg g^{-1}), which depends on the number of adsorption sites.

After linearization of the Langmuir isotherm, eqn (2), we obtain:

$$\frac{C_e}{q_e} = \frac{1}{bQ_0} + \frac{C_e}{Q_0} \quad (2)$$

The values of Q_0 and b are calculated from the slope and intercept of the plot of C_e/q_e *vs.* C_e for MSP NPs and MP NPs (Fig. S8†).

The Freundlich isotherm model is an empirical equation that describes the surface heterogeneity of the sorbent. It considers multilayer adsorption with a heterogeneous energetic distribution of active sites, accompanied by interactions between adsorbed molecules.[60] The Freundlich empirical model is represented by:

$$q_e = K_f C_e^{1/n} \quad (3)$$

where C_e is the equilibrium concentration (mg mL^{-1}), q_e is the amount adsorbed at equilibrium (mg g^{-1}), and K_f (mg$^{1-1/n}$ mL$^{1/n}$ g^{-1}) and $1/n$ are Freundlich constants depending on the temperature and the given adsorbent–adsorbate couple. n is related to the adsorption energy distribution, and K_f indicates

the adsorption capacity. The linearized form of the Freundlich adsorption isotherm equation[63] is

$$\ln q_e = \ln K_f + \left(\frac{1}{n}\right)\ln C_e \quad (4)$$

The values of K_f (mL g^{-1}) and $1/n$ are calculated from the intercept and slope of the plot of ln q_e *vs.* ln C_e for MSP NPs and MP NPs (Fig. S9†).

The Redlich–Peterson isotherm unites the Langmuir and Freundlich isotherms, it describes adsorption on heterogeneous surfaces, as it contains the heterogeneity factor β. This equation has three parameters, K_{RP} is the constant of Redlich–Peterson isotherm (mL g^{-1}), α_{RP} is the Redlich–Peterson constant (mL mg^{-1}), and β is the Redlich–Peterson exponent ($0 < \beta < 1$). It can be reduced to the Langmuir equation as β approaches 1.[61,64] The general equation can be described as follows[61,65]

$$\frac{K_{RP}C_e}{1 + \alpha_{RP}C^{\beta}} \quad (5)$$

or

$$q_e = \frac{Q'_{mon}\,\alpha_{RP}\,C_e}{1 + \alpha_{RP}C^{\beta}} \quad (6)$$

where C_e is the equilibrium concentration (mg mL^{-1}), q_e is the amount adsorbed at equilibrium (mg g^{-1}) and Q'_{mon} is the Redlich–Peterson maximum adsorption capacity (mg g^{-1}). K_{RP} is the product of Q'_{mon} and α_{RP}.

According to Wu *et al.*,[65] a linear form of eqn (6) can be transformed as

$$\frac{q_e}{C_e} = \frac{1}{Q'_{mon}\alpha_{RP}} + \frac{1}{Q'_{mon}}C_e^{\beta} \quad (7)$$

The Redlich–Peterson isotherm curves of the model dyes are presented in Fig. S10† using the plot of q_e/C_e *vs.* C_e^{β} for MSP NPs and MP NPs.

Sips developed a new model as an improvement to the Freundlich and Langmuir equations.[66] This model is based on the Freundlich equation assumption, where the amount of adsorbed dye increases with the increase of initial concentration, but Sips equation presumes that the adsorption capacity has a finite limit when the concentration is sufficiently high.[67] The Sips[62] equation can be represented as follows;

$$q_e = \frac{Q_m K_s\, C_e^{1/n}}{1 + K_s C_e^{1/n}} \quad (8)$$

Table 6 Maximum adsorption capacities (Q_0 in mg g^{-1}) and kinetic models for the model dyes by some other adsorbents reported in literature

	Capacity factor (Q_0 (mg g^{-1}))					
Sorbent	CV	MB	EBT	MO	Kinetic models	Ref.
Fe_3O_4@APS@AA-*co*-CA MNPs	208	142.9	—	—	Pseudo 2nd order	71
Magnetic-modified multi-walled carbon nanotubes	227	48.1	—	—	—	72
Magnetic nanocomposite	81	—	—	—	—	73
MWCNTs/$Mn_{0.8}Zn_{0.2}Fe_2O_4$ composite	5	—	—	—	Pseudo 2nd order	74
N-Benzyl-*O*-carboxymethylchitosan magnetic NPs	248	223.58	—	—	Pseudo 2nd order	54
Magnetite nanoparticles loaded tea waste (MNLTW)	113.69	119	—	—	Pseudo 2nd order	75
Graphene nanosheet (GNS)/magnetite (Fe_3O_4) composite	—	43.82	—	—	Pseudo 2nd order	76
Poly(c-glutamic acid) (PGA-MNPs)	—	78.67	—	—	Pseudo 2nd order	5
Montmorillonite clay modified with iron oxide (MtMIO)	—	71.2	—	—	Pseudo 2nd order	77
Fe_3O_4 NPs coated with pectin and crosslinked with adipic acid (FN-PAA)	—	221.7	—	—	Pseudo 2nd order	6
Eucalyptus bark	—	—	52.37	—	Pseudo 1st order	78
Scolymus hispanicus L.	—	237.18	120.42	—	Pseudo 2nd order	79
$NiFe_2O_4$ nanoparticles	—	—	47	—	Pseudo 2nd order	80
Nteje clay			16.26		Pseudo 2nd order	81
Activated carbon modified by silver nanoparticles	—	—	—	0.69	Pseudo 2nd order	82
Ash *Moringa peregrina*	—	—	—	15.43	—	83
Dragon fruit (Hylocereusundatus) foliage	—	—	—	17.67	Pseudo 2nd order	84
Chitosan intercalated montmorillonite	—	—	—	70.42	Pseudo 2nd order	85
Silica gel waste (SGW), modified with cationic surfactant	—	—	—	45.45	Pseudo 2nd order	86
Polyaniline modified ZnO	—	—	—	28.94	Pseudo 1st order	87
Magnetite/pectin NPs	100	125	103.41	47.36	Pseudo 2nd order	Present work
Magnetite/silica/pectin NPs	125	178.57	80.15	27.74	Pseudo 2nd order	Present work

where Q_m is the maximum adsorption capacity calculated by Sips (mg g^{-1}), K_s is the Sips constant (mL mg^{-1}) and n is the Sips model exponent.

The Sips isotherm curves of the model dyes are presented in Fig. S11† using the plot of q_e *vs.* $C_e^{1/n}$ for MSP NPs and MP NPs.

The parameters of Langmuir, Freundlich, Redlich–Peterson and Sips equations are listed in Table 5 for MSP and MP NPs. For both of MSP and MP NPs, the values of correlation coefficient, R^2, and Chi square (χ^2) for the fit of experimental isotherm data to equation are the best for Sips model. Such results indicate that the adsorption process of model dyes is going on after a combined model Freundlich and Langmuir: diffused adsorption on low dye concentration, and a monomolecular adsorption with a saturation value at high adsorbate concentrations.[66,68,69] Additionally, the values of $1/n$ for Sips isotherm are $0 < 1/n < 1$, indicating that the dyes adsorption process is favorable.

The Q_m values were calculated form the Sips isotherm for cationic dyes at optimum pH (~8) for MP and MSP NPs and were estimated to be (CV = 140.49 mg g^{-1}, MB = 168.72 mg g^{-1}) and (CV = 180.29 mg g^{-1}, MB = 197.18 mg g^{-1}), respectively. For the anionic dyes, the Q_m values calculated at optimum pH (~2) for MP and MSP NPs were estimated to be (EBT = 72.35 mg g^{-1}, MO = 27.215 mg g^{-1}) and (EBT = 65.35 mg g^{-1}, MO = 2 6.754 mg g^{-1}), respectively. This data indicates that our proposed adsorbents (MSP NPs and MP NPs) can be considered promising materials for the removal of cationic and anionic dyes from aqueous solution.

Generally, isotherms relating solid-phase to fluid-phase concentration for adsorption of a single component directly influence the behavior of the isotherm curves.[70] The elucidation relating the isotherm curves and the equilibrium behavior is given by a dimensionless "separation factor" or "equilibrium parameter", (R_L) which is presented by eqn (9):

$$R_L = 1/(1 + bC_0) \quad (9)$$

where C_0 (mg mL^{-1}) is the initial solute concentration and b is the equilibrium constant obtained from the Langmuir curve. R_L values within the range $0 < R_L < 1$ indicate favorable adsorption.[70] Accordingly, by substituting the b values for the present adsorption systems, the R_L values obtained with initial dyes concentration of 200 mg L^{-1} ranged between (0.11 and 0.69) and thus indicate favorable adsorption of the model dyes onto the NPs.

3.3.6. Evaluation of performance. The maximum adsorption capacities (Q_m) and the kinetic model of MP and MSP nanoparticles together with other magnetic, residue and bio-based adsorbents reported in the literature for CV, MB, EBT and MO adsorption at ambient temperature are listed in Table 6. The Q_m for our MP NPs and MSP NPs are higher than that for general adsorbents used for the model dyes. However,

Table 7 Pseudo-first order, and pseudo-second-order kinetic models parameters for the adsorption of model dyes by MSP NPs

	Pseudo 1st order					Pseudo 2nd order				Intraparticle diffusion			
	q_e (exp) (mg g^{-1})	q_e (cal) (mg g^{-1})	K_1 (h^{-1})	R^2	χ^2	q_e (cal) (mg g^{-1})	K_2 (mg g^{-1} h^{-1})	R^2	χ^2	K_{id}	C	R^2	χ^2
CV													
10 mg L^{-1}	9.94	5.93	2.612	0.9308	0.252	10.56	0.760	0.9976	0.207	0.376	6.174	0.8918	0.138
50 mg L^{-1}	36.51	10.15	1.912	0.9311	0.039	37.45	0.419	0.9997	0.118	0.878	27.563	0.8865	0.205
100 mg L^{-1}	64.94	14.87	2.501	0.949	0.129	66.23	0.380	0.9998	0.175	1.047	54.551	0.8459	0.222
150 mg L^{-1}	78.61	15.74	1.275	0.9701	0.058	80	0.195	0.9992	1.374	1.563	61.505	0.9705	0.067
200 mg L^{-1}	90.29	31.12	2.873	0.9669	0.081	93.46	0.164	0.9998	0.243	2.389	67.356	0.843	0.857
MB													
10 mg L^{-1}	12.84	2.89	3.195	0.9756	0.026	13.09	2.335	0.9998	0.049	0.194	10.988	0.7994	0.051
50 mg L^{-1}	66.07	12.24	1.137	0.9607	0.202	66.67	0.25	0.9992	0.533	1.338	51.386	0.9089	0.207
100 mg L^{-1}	107.58	23.65	1.928	0.9615	0.107	109.89	0.166	0.9998	1.111	1.889	88.125	0.9435	0.145
150 mg L^{-1}	132.61	27.44	1.688	0.7998	0.498	135.14	0.137	0.9993	2.895	1.982	110.85	0.9722	0.061
200 mg L^{-1}	151.16	40.5	2.004	0.9277	0.356	153.85	0.106	0.9996	1.18	3.469	116.06	0.8559	0.999
EBT													
10 mg L^{-1}	9.23	10.23	2.553	0.8951	2.073	10.41	0.368	0.9977	0.123	0.571	3.423	0.9572	0.146
50 mg L^{-1}	29.22	18.06	2.444	0.9728	0.148	31.25	0.233	0.9997	0.062	11.336	16.048	0.8601	0.843
100 mg L^{-1}	38.64	19.25	2.225	0.9648	0.479	40.98	0.198	0.9993	0.146	1.674	22.213	0.8005	1.534
150 mg L^{-1}	59.64	23.05	1.951	0.9715	1.627	62.5	0.151	0.9995	0.431	2.39	36.025	0.7583	2.605
200 mg L^{-1}	76.09	26.47	1.56	0.9557	0.093	78.74	0.124	0.9989	1.112	2.393	50.712	0.9596	0.254
MO													
10 mg L^{-1}	2.19	2.95	2.313	0.9221	1.58	2.77	0.695	0.9994	0.002	0.188	0.276	0.9653	0.064
50 mg L^{-1}	9.26	5.28	1.796	0.9499	0.078	9.91	0.583	0.9979	0.226	0.422	4.831	0.9777	0.038
100 mg L^{-1}	13.54	5.95	1.953	0.9632	0.075	14.39	0.525	0.9992	0.104	0.589	7.659	0.8898	0.247
150 mg L^{-1}	22.46	10.46	2.011	0.9618	0.101	23.58	0.367	0.9992	0.255	0.804	14.213	0.9445	0.138
200 mg L^{-1}	25.78	10.39	2.047	0.9905	0.249	27.03	0.351	0.9999	0.014	0.997	15.932	0.824	0.679

Table 8 Pseudo-first order, and pseudo-second-order kinetic models parameters for the adsorption of model dyes by MP NPs

	Pseudo 1st order					Pseudo 2nd order				Intraparticle diffusion			
	q_e (exp) (mg g^{-1})	q_e (cal) (mg g^{-1})	K_1 (h^{-1})	R^2	χ^2	q_e (cal) (mg g^{-1})	K_2 (mg g^{-1} h^{-1})	R^2	χ^2	K_{id} (mg g^{-1} min$^{-0.5}$)	C (L)	R^2	χ^2
CV													
10 mg L^{-1}	10.46	5.81	1.865	0.9747	0.039	11.22	0.526	0.9994	0.036	0.514	5.22	0.9107	0.221
50 mg L^{-1}	37.59	7.32	1.349	0.9365	0.091	38.17	0.458	0.9995	0.202	0.782	29.279	0.983	2.058
100 mg L^{-1}	62.49	2.64	2.854	0.9495	0.008	62.89	0.396	1	0.016	0.239	60.221	0.7656	0.019
150 mg L^{-1}	72.45	10.83	2.538	0.787	0.535	73.53	0.369	0.9993	0.454	1.058	62.1	0.6501	0.597
200 mg L^{-1}	78.04	12.59	3.318	0.8498	1.886	80	0.313	0.9996	0.482	1.754	61.859	0.6415	1.605
MB													
10 mg L^{-1}	14.01	13.09	3.399	0.9503	1.127	14.93	0.561	0.9997	0.044	0.585	8.315	0.8837	0.252
50 mg L^{-1}	41.12	14.47	1.322	0.9641	0.125	42.55	0.19	0.9971	1.824	1.311	26.59	0.9879	0.039
100 mg L^{-1}	66.36	24.11	1.651	0.9475	0.425	68.97	0.162	0.9992	0.948	1.915	46.471	0.9551	0.201
150 mg L^{-1}	72.54	27.15	2.065	0.9388	0.172	75.19	0.147	0.9995	0.457	2.179	50.442	0.89	0.639
200 mg L^{-1}	81.15	19.25	1.065	0.8945	0.303	81.97	0.135	0.9968	4.532	1.657	61.337	0.9579	0.108
EBT													
10 mg L^{-1}	9.98	5.51	1.686	0.9786	0.044	10.72	0.503	0.9982	0.112	0.495	4.828	0.94	0.143
50 mg L^{-1}	35.74	13.72	1.703	0.9001	0.509	37.17	0.278	0.9976	1.377	1.01	24.753	0.9798	0.046
100 mg L^{-1}	52.11	15.25	1.698	0.9195	0.206	53.48	0.233	0.999	1.439	1.195	39.312	0.9821	0.037
150 mg L^{-1}	70.93	20.75	1.996	0.9641	0.367	72.99	0.209	0.9994	1.311	1.515	55.178	0.9682	0.076
200 mg L^{-1}	92.29	16.32	1.394	0.8998	0.579	93.46	0.191	0.9997	0.351	2.01	71.637	0.835	0.639
MO													
10 mg L^{-1}	3.28	1.39	1.529	0.9895	0.016	3.46	1.985	0.999	0.032	0.14	1.814	0.928	0.04
50 mg L^{-1}	13.68	8.04	2.251	0.9556	0.187	14.64	0.491	0.999	0.229	0.562	7.979	0.9553	0.084
100 mg L^{-1}	21.32	8.52	2.284	0.9745	0.086	22.32	0.478	0.9997	0.102	0.761	13.875	0.8347	0.413
150 mg L^{-1}	34.63	17.97	1.941	0.9506	0.149	36.63	0.196	0.999	0.466	1.43	19.917	0.9417	0.302
200 mg L^{-1}	45.62	21.88	2.027	0.9167	0.269	47.85	0.182	0.9991	0.544	1.625	28.875	0.9462	0.265

adsorption capacities are low compared to some adsorbents including magnetic modified MWCNTs and *N*-benzyl-*O*-carboxymethylchitosan magnetic NPs for CV, Fe_3O_4 NPs coated with pectin and crosslinked with adipic acid (FN-PAA) for MB, *Scolymus hispanicus* L. bacteria for EBT and chitosan intercalated montmorillonite for MO. Such results do not diminish the feasibility of employing MP NPs and MSP NPs as adsorbents for dye removal from aqueous solutions, since they were advantageous in presenting good adsorption capacity in comparison to other newly proposed adsorbents for all types of dyes (anionic and cationic dyes). Moreover, MP NPs and MSP NPs are superior to other adsorbents in terms of simplicity of the preparation method and separation procedures, causing little environmental pollution and having a reusable characteristic.

3.3.7. Adsorption kinetics. The adsorption kinetic models were applied to interpret the experimental data to determine the controlling mechanism of dye adsorption from aqueous solution. Here, pseudo-first-order and pseudo-second-order model were used to test dynamical experimental data.[88] The pseudo-first order kinetic model of Lagergren[89] is given by:

$$\log(q_1 - q_t) = \log q_{1e} - \frac{K_1 t}{2.303} \quad (10)$$

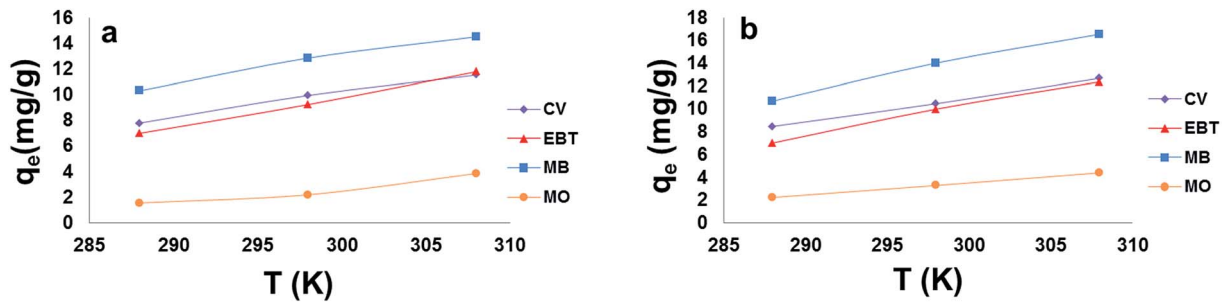

Fig. 10 Effect of temperature on the adsorption capacity (q_e) of model dyes onto; [a] MSP NPs and [b] MP NPs. Adsorbent: 5 g L^{-1}, dyes 10 mg L^{-1}, pH: 2.0 for anionic dyes and 8.0 for cationic dyes, time: 120 min. Magnetite/Pectin Nanoparticles: MP NPs and Magnetite/Silica/Pectin Nanoparticles: MSP NPs.

where q_t is the amount of dye adsorbed per unit of adsorbent (mg g^{-1}) at time t, K_1 is the pseudo-first order rate constant (h^{-1}). The adsorption rate constant (K_1) were calculated from the plot of $\log(q_e - q_t)$ against t.

Ho and McKay[90] presented the pseudo-second order kinetic as:

$$\frac{t}{q_t} = \frac{1}{K_2 q_e^2} + \frac{t}{q_e} \quad (11)$$

where K_2 is the pseudo-second order rate constant (g mg^{-1} h^{-1}). The q_e and K_2 can be obtained by linear plot of t/q_t *versus* t.

Fig. S12 and S13† are the plots of the pseudo-first order and second order kinetics of model dyes adsorption on MSP respectively. Fig. S15 and S16† are the plots of the pseudo-first order and second order kinetics of model dyes adsorption on MP NPs respectively. The calculated kinetic parameters are given in Tables 7 and 8 for MSP NPs and MP NPs respectively.

In all model dyes, the correlation coefficient for the pseudo-first-order model (Fig. S12 and S15†) is relatively low, the calculated q_e value (q_{1e}) obtained from this equation does not give reasonable value (Tables 7 and 8), which is much lower than experimental data ($q_{e,exp}$). This result suggests that the adsorption process does not follow the pseudo-first-order kinetic model. On the contrary, the results present an ideal fit to the second order kinetic for adsorbent with the extremely high $r^2 \geq 0.999$ (Fig. S13 and S16†). A good agreement with this adsorption model is confirmed by the similar values of calculated q_e for second order kinetic and the experimental ones for adsorbents. The best fit to the pseudo-second order kinetics indicates that the adsorption mechanism depends on the adsorbate and adsorbent. Such results come in accordance with other literature as listed in Table 6.

3.3.8. Intra-particle diffusion model. The experimental data was further investigated by the diffusion (intra-particle) model to explain the diffusion mechanism. The plots (q_t *vs.* $t^{0.5}$) represent multi-linearity, which indicates two or more steps occurring in the adsorption process.[35] The relationship between q_t *vs.* $t^{0.5}$ is plotted in Fig. S13 and S16† for MSP NPs and MP NPs respectively. The intra-particle diffusion constant and the boundary layer thickness were calculated using the linear equation (Tables 7 and 8).

$$q_t = K_{id} t^{0.5} + C \quad (12)$$

where q_t is the amount of dye adsorbed onto the adsorbent at time t (mg g^{-1}), C is the boundary layer thickness, and K_{id} is the intra-particle diffusion rate constant (mg g^{-1} $min^{-0.5}$).

If plot (q_t *vs.* $t^{0.5}$) is straight line passing from origin, then intra-particle diffusion becomes rate-limiting step. As can be observed from Fig. S14 and S17,† the plots are not linear over the whole time range which means that the intraparticle diffusion is not the rate determining step of the adsorption mechanism of the model dyes onto MSP NPs and MP NPs.[67,91] The values of intercept (Tables 7 and 8) give an idea about the boundary layer thickness, *i.e.*, the larger intercept the greater is the boundary layer effect and this means that the adsorption is more boundary layer controlled.[67,92]

Table 9 Thermodynamic parameters for the adsorption of model dyes on MSP NPs and MP NPs

	T (K)	K_0	ΔG° (kJ mol^{-1})	ΔH° (kJ mol^{-1})	ΔS° (J mol^{-1} K)	R^2
MSP NPs						
CV	288	1.4426	−0.9113	30.034	107.45	0.9961
	298	2.2956	−1.9858			
	308	3.2542	−3.06			
MB	288	3.0655	−2.621	48.788	178.751	0.9999
	298	6.1435	−4.4796			
	308	11.5079	−6.2671			
EBT	288	0.8904	0.2978	32.747	112.671	0.9989
	298	1.3735	−0.8289			
	308	2.1654	−1.9556			
MO	288	0.1655	6.0877	38.298	111.84	0.9700
	298	0.2423	4.9693			
	308	0.4695	3.8509			
MP NPs						
CV	288	1.4405	−0.8412	31.429	112.048	0.9965
	298	2.1434	−1.9617			
	308	3.8133	−3.0821			
MB	288	1.9651	−1.6249	44.477	160.078	0.9999
	298	3.6966	−3.2257			
	308	6.5635	−4.8265			
EBT	288	0.9589	0.0611	37.824	131.12	0.9968
	298	1.7118	−1.2501			
	308	2.6717	−2.5613			
MO	288	0.2528	3.2692	29.771	92.019	0.998
	298	0.3957	2.2349			
	308	0.5665	1.4288			

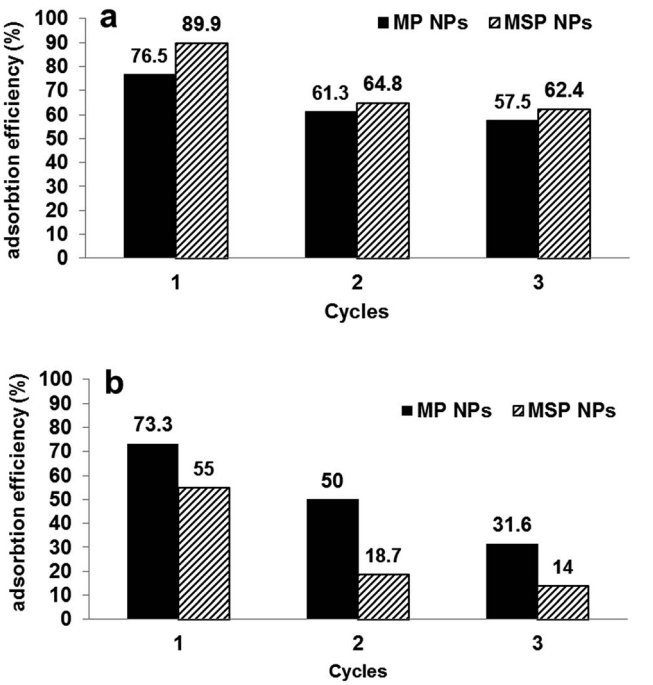

Fig. 11 Performance of magnetite/pectin NPs (MP NPs) and magnetite/silica/pectin NPs (MSP NPs) by three cycles of adsorption/desorption for [a] methylene blue and [b] Eriochrome black T.

3.3.9. Thermodynamic studies. Evaluation of temperature was carried out with the scope of testing the ability of MSP NPs and MP NPs in dyes removal in different circumstances according to a previous method.[79] Data were collected at three temperatures: from 288 to 308 K. The variation of the model dyes (CV, MB, EBT and MO) adsorbed on MSP NPs and MP NPs as function of solution temperature is shown in Fig. 10. An increase of the amount of dyes adsorbed was observed when the temperature increases. From these results, thermodynamic parameters including the change in free energy (ΔG°), enthalpy (ΔH°) and entropy (ΔS°) were used to describe thermodynamic behavior of the adsorption of the model dyes onto MSP NPs and MP NPs. These parameters were calculated using the following equations

$$\Delta G^\circ = -RT \ln K \quad (13)$$

$$K = \frac{q_e}{C_e} \quad (14)$$

$$\ln K = \frac{\Delta S^\circ}{R} - \frac{\Delta H^\circ}{RT} \quad (15)$$

$$\Delta G^\circ = \Delta H^\circ - T\Delta S^\circ \quad (16)$$

where K is the equilibrium constant, R is the universal gas constant (8.314 J mol^{-1} K^{-1}), T is temperature (K), q_e is the amount of dye adsorbed on the adsorbents per liter of the solution at equilibrium (mg L^{-1}), C_e is the equilibrium concentration of the dye in the solution (mg L^{-1}).

The enthalpy (ΔH°) and entropy (ΔS°) of adsorption were estimated from the slope and intercept of the plot of ln K *versus* $1/T$ yields, respectively.

The ΔH° and ΔS° values are presented in Table 9. The values are within the range of 1 to 83 kJ mol^{-1} and indicate the favorability of physisorption.[93] The positive values of ΔH° show the endothermic nature of adsorption and also indicate the possibility of physical adsorption.[93–97] The negative values of ΔG° (Table 9) show that adsorption is highly favorable for MB, CV and EBT dyes while MO showed positive values of ΔG°. Such result indicates that the MB, CV and EBT dyes adsorption was spontaneous. The positive values of ΔS° (Table 9) show the increased disorder and randomness at the solid solution interface during the adsorption of dyes on the adsorbents.[67]

Enhancement of adsorption capacity of MSP NPs and MPs NPs at higher temperatures may be attributed to the increase in the mobility of the large dye ion with temperature. An increasing number of molecules may also acquire sufficient energy to undergo an interaction with active sites at the surface.[92]

3.4. Desorption and regeneration studies

The magnetite/pectin NPs and magnetite/silica pectin NPs have good performance in recycling treatment with cationic dyes. Our adsorbents did not significantly adsorb cationic dyes at pH < 3.0 (Fig. 8), which suggests that the adsorbed cationic dyes may be desorbed in solution with such pH values.[98] In addition, organic cationic dyes dissolved easily in organic solvents. Thus, desorption of the cationic methylene blue dye was demonstrated with 50 mL mixture of 5% (v/v) acetic acid and methanol,[71] for which about 90.0% of desorption efficiency was achieved. The results of adsorption efficiency of the studied adsorbents after three cycles are shown in Fig. 11[a]. The efficiency of adsorption decreased to two thirds after the 1st cycle and remained nearly constant throughout the 2nd and 3rd cycle for both types of adsorbents.

Desorption–adsorption experiments have also been performed to evaluate the possibility of regeneration and reuse of the adsorbents for removal of anionic dyes (EBT was taken as an example). As the results show in Fig. 11[b], adsorption efficiencies were decreased by 25% from that achieved in the 1st cycle and 20% from that of the 2nd cycle. Nearly same results were obtained when using methanol alone and mixture of 5% (v/v) NaOH and methanol for EBT regeneration which elucidates that the reusability of the sorbents was better in removal of cationic dyes than in the case of anionic dyes.

3.5. Dye mixture adsorption studies

The selectivity of MP NPs and MSP NPs towards cationic and anionic dyes was investigated with initial dyes' concentration fixed at 165 mg L^{-1} for each dye and 2 g L^{-1} adsorbents mass. In former single dye adsorption studies, pH showed significant

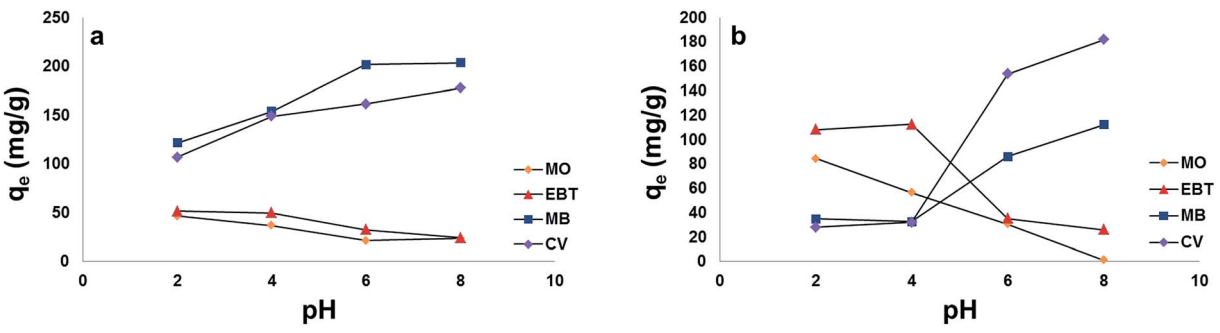

Fig. 12 Effect of pH on the adsorption capacity (q_e) of model dyes in their mixture solutions onto; [a] MSP NPs and [b] MP NPs. Adsorbent: 2 g L^{-1}, dyes 165 mg L^{-1}, temperature: 25 °C, time: 120 min. Magnetite/Pectin Nanoparticles: MP NPs and Magnetite/Silica/Pectin Nanoparticles: MSP NPs.

effect on the efficiency of adsorption of cationic and anionic dyes onto MP and MSP NPs. Thus the effect of pH in the range 2–8 on the removal of the model dyes mixtures (MB, CV, EBT and MO) was studied.

As Fig. 12[a] and [b] show, the results agree with those obtained in the previous single dye adsorption experiments measured spectrophotometrically. For the cationic dyes (MB and CV) the adsorption was remarkably decreased in pH 2.0. The capacity of dye adsorption for MB and CV increased with increasing the solution pH from 2.0 to 8.0, reaching its maximum at 8. For the anionic dyes (MO and EBT), as observed in Fig. 12[a] and [b], the adsorption is high in acidic medium and decreases with the increase in solution pH.

Moreover, higher adsorption capacities (q_e) of cationic dyes on MSP NPs (MB = 203.4 mg g^{-1} and CV = 177.5 mg g^{-1}) were observed than that on MP NPs (MB = 112.2 mg g^{-1} and CV = 181.8 mg g^{-1}). This also comes in agreement with the results obtained from the single dyes adsorption experiments. On the other hand, since the MP NPs offers a lesser negatively charged surface than MSP NPs in acidic pH, it favors the adsorption of anionic dyes (q_e of MO = 84.4 mg g^{-1} and q_e of EBT = 108.3 mg g^{-1}) than that of MSP NPs (q_e of MO = 46.5 mg g^{-1} and q_e of EBT = 51.5 mg g^{-1}).

Simultaneous adsorption of the model dyes onto MSP NPs and MP NPs was tested at natural pH of samples (pH $\approx$ 6) without pH adjustment as a trial for large scale wastewater treatment application. MSP NPs and MP NPs showed more adsorption towards cationic dyes (q_e ranging between 86 and 201 mg g^{-1}) than the anionic ones (q_e ranging between 21 and 35 mg g^{-1}). Such findings can be attributed to the negatively charged surface of the NPs at elevated pHs that attracts the positively charged dye molecules. Thus our proposed NPs can be applied for wastewater treatment and the removal of cationic dyes at natural pH of water samples.

4. Conclusion

In this study, we compared the physical and chemical properties of pectin coated magnetite nanoparticles prepared *via* two different co-precipitation techniques using data obtained by TEM, XRD, FTIR, VSM and zeta potential. Both coated NPs showed alteration in shape and particle size as indicated by TEM images which means we can have a control over the size of particles *via* pectin coating. FTIR spectra elucidated the successful pectin coating on magnetite and magnetite/silica NPs surfaces *via* carboxylate linkage. The pure magnetite phase formation was indicated by XRD data of MP NPs but upon increasing pectin concentration up to 1 w/v% other phases appeared. On the other hand, the double shell MSP NPs kept the pure magnetite phase in all prepared samples which indicated that the coating didn't affect the crystal structure of the nanoparticles. The VSM data of the MSP NPs also elucidated a minor decrease in the M_s of coated samples in comparison to the uncoated ones which indicates that the silica/pectin coating didn't cause much alteration in the NPs' magnetic properties. Yet, a great decrease in the saturation magnetization of MP NPs was observed with increasing pectin concentration. Moreover, MSP NPs had better dispersion properties than the MP NPs where the latter formed some aggregates especially in the high pectin concentration samples.

The adsorption potential of MP NPs and MSP NPs was investigated for the removal of cationic and anionic dyes from aqueous systems. The effects of contact time, initial dye concentrations, pH and adsorbent mass on the adsorption process and desorption were discussed. Analysis was done using validated spectrophotometric and chromatographic methods. Adsorption kinetics was fitted with the pseudo-second-order model, and adsorption isotherms were described by Langmuir, Freundlich, Redlich–Peterson and Sips equation. The adsorption mechanism of the model dyes onto the proposed adsorbents was based on electrostatic force of attraction between cationic and anionic dyes and the adsorbents upon adjustment of pH. Regeneration of MP NPs and MSP NPs by methanol was done in order to reuse them for successive removal processes with high removal efficiency.

Simultaneous adsorption of the cationic and anionic dyes onto MSP NPs and MP NPs from dye mixture solution was tested as a trial for large scale wastewater treatment application. Higher adsorption capacities of cationic dyes on MSP NPs were observed while MP NPs favored the adsorption of anionic dyes.

In conclusion, MSP NPs and MP NPs are promising alternatives for cationic and anionic dyes removal from wastewater because of their high adsorption capacities and separation convenience. We believe that the approach presented herein can provide a convenient way to bind other cationic and anionic organic compound or heavy metal ions to our magnetic absorbents and to quickly separate them from wastewater.

Acknowledgements

This research was supported by science and technology development fund (STDF), Egypt. Project number 12641.

References

1 L. Ai, C. Zhang, F. Liao, Y. Wang and M. Li, *J. Hazard. Mater.*, 2011, **198**, 282–290.
2 O. Legrini, E. Oliveros and A. Braun, *Chem. Rev.*, 1993, **93**, 671–698.
3 S. Li, *Bioresour. Technol.*, 2010, **101**, 2197–2202.
4 N. Bao, Y. Li, Z. Wei, G. Yin and J. Niu, *J. Phys. Chem. C*, 2011, **115**, 5708–5719.
5 B. Inbaraj and B. Chen, *Bioresour. Technol.*, 2011, **102**, 8868–8876.
6 R. Rakhshaee and M. Panahandeh, *J. Hazard. Mater.*, 2011, **189**, 158–166.
7 P. S. Guru and S. Dash, *J. Dispersion Sci. Technol.*, 2012, **33**, 1012–1020.
8 S. Oh, D. Cha, P. Chiu and B. Kim, *Water Sci. Technol.*, 2004, **49**, 129–136.
9 J. Perey, P. Chiu, C. Huang and D. Cha, *Water Environ. Res.*, 2002, **74**, 221–225.
10 A. Afkhami and R. Moosavi, *J. Hazard. Mater.*, 2010, **174**, 398–403.

11 C. Yavuz, J. Mayo, W. William and A. Prakash, *Science*, 2006, **314**, 964–967.
12 A. Afkhami, M. Saber-Tehrani and H. Bagheri, *Desalination*, 2010, **263**, 240–248.
13 A. Gupta and M. Gupta, *Biomaterials*, 2005, **26**, 3995–4021.
14 S. Mak and D. Chen, *Dyes Pigm.*, 2004, **61**, 93–98.
15 S. Huang and D. Chen, *J. Hazard. Mater.*, 2009, **163**, 174–179.
16 S. Banerjee and D. Chen, *J. Hazard. Mater.*, 2007, **147**, 792–799.
17 C. Vilhena, M. Goncalves and A. Mota, *Electroanalysis*, 2004, **16**, 2065–2072.
18 GITCO, 1999.
19 A. Konno, M. Miyawaki, M. Misaki and K. Yasumatsu, *Agric. Biol. Chem.*, 2014, **45**, 2341–2342.
20 A. Madhav, M.Sc. thesis, Kerala Agricultural University, Thrissur, 2001, p. 52.
21 A. Cucheval, M. A. Al-Ghobashy, Y. Hemar, D. Otter and M. A. K. Williams, *J. Colloid Interface Sci.*, 2009, **338**, 450–462.
22 A. A. S. Raj and T. V. Ranganathan, *Sci. Rep.*, 2012, **1**, 553, DOI: 10.4172/scientificreports.553.
23 Y. Lin, C. Weng and F. Chen, *Sep. Purif. Technol.*, 2008, **64**, 26–30.
24 F.-T. J. Ngenefeme, N. J. Eko, Y. D. Mbom, N. D. Tantoh and K. W. M. Rui, *Open J. Compos. Mater.*, 2013, **03**, 30–37.
25 http://www.wiredchemist.com/chemistry/data/acid-base-indicators, accessed at October 12, 2015.
26 http://www.chemicalbook.com/, accessed at October 12, 2015.
27 http://pubchem.ncbi.nlm.nih.gov/, accessed at October 12, 2015.
28 http://en.wikipedia.org/wiki/, accessed at October 12, 2015.
29 *International Conference on Harmonization (ICH), Q2B, Validation of Analytical Procedures*, US FDA Federal Register, 1994, accessed at October 12, 2015.
30 *International Conference on Harmonization (ICH), Q2, Validation of Analytical Procedures*, 2005.
31 *International Conference on Harmonization (ICH), Q2B, Validation of Analytical Procedures: Definitions and Terminology*, US FDA Federal Register, 1995, vol. 60.
32 J.-L. Gong, X.-Y. Wang, G.-M. Zeng, L. Chen, J.-H. Deng, X.-R. Zhang and Q.-Y. Niu, *Chem. Eng. J.*, 2012, **185–186**, 100–107.
33 Z. Lei, X. Pang, N. Li, L. Lin and Y. Li, *J. Mater. Process. Technol.*, 2009, **209**, 3218–3225.
34 M. Seenuvasan, C. G. Malar, S. Preethi, N. Balaji, J. Iyyappan, M. A. Kumar and K. S. Kumar, *Mater. Sci. Eng., C*, 2013, **33**, 2273–2279.
35 Markandeya, S. P. Shukla and G. C. Kisku, *Res. J. Environ. Toxicol.*, 2015, **9**, 320–331.
36 D. Confortin, H. Neevel, M. Brustolon, L. Franco, A. J. Kettelarij, R. M. Williams and M. R. van Bommel, *J. Phys.: Conf. Ser.*, 2010, **231**, 012011.
37 U. The United States Pharmacopoeia & National Formulary, US Pharmacopoeial Convention Inc., 2011.
38 W. H. Organization, *The International Pharmacopoeia*, World Health Organization, 2006, vol. 1.
39 A. Bee, R. Massart and S. Neveu, *J. Magn. Magn. Mater.*, 1995, **149**, 6–9.
40 S. Liang, X. Guo, N. Feng and Q. Tian, *J. Hazard. Mater.*, 2010, **174**, 756–762.
41 T. T. Baby and S. Ramaprabhu, *Talanta*, 2010, **80**, 2016–2022.
42 J. Liu, Z. Zhao and G. Jiang, *Environ. Sci. Technol.*, 2008, **42**, 6949–6954.
43 D. Predoi, R. Clerac, A. Jitianu, M. Zaharescu, M. Crisan and M. Raileanu, *Digest Journal of Nanomaterials and Biostructures*, 2006, **1**, 93–97.
44 E. V. Escobar Zapata, C. A. Martínez Pérez, C. A. Rodríguez González, J. S. Castro Carmona, M. A. Quevedo Lopez and P. E. García-Casillas, *J. Alloys Compd.*, 2012, **536**, S441–S444.
45 A. L. Andrade, D. M. Souza, M. C. Pereira, J. D. Fabris and R. Z. Domingues, *Ceramica*, 2009, **55**, 420–424.
46 M. Mikhaylova, D. K. Kim, N. Bobrysheva, M. Osmolowsky, V. Semenov, T. Tsakalakos and M. Muhammed, *Langmuir*, 2004, **20**, 2472–2477.
47 Z. Ma, Y. Guan and H. Liu, *J. Polym. Sci., Part A: Polym. Chem.*, 2005, **43**, 3433–3439.
48 R. K. Dutta and S. Sahu, *Eur. J. Pharm. Biopharm.*, 2012, **82**, 58–65.
49 S. Theerdhala, D. Bahadur, S. Vitta, N. Perkas, Z. Zhong and A. Gedanken, *Ultrason. Sonochem.*, 2010, **17**, 730–737.
50 R. M. Cornell and V. Schwertmann, *The Iron Oxides: Structure, Properties, Reactions, Occurrence and Uses*, VCH Publishers, Weinheim, 2nd edn, 2003.
51 S. K. Giri, N. N. Das and G. C. Pradhan, *Colloids Surf., A*, 2011, **389**, 43–49.
52 M. Szekeres, I. Y. Tóth, E. Illés, A. Hajdú, I. Zupkó, K. Farkas, G. Oszlánczi, L. Tiszlavicz and E. Tombácz, *Int. J. Mol. Sci.*, 2013, **14**, 14550–14574.
53 R. H. Müller and G. E. Hildebrand, *J. Drug Targeting*, 1996, **4**, 161–170.
54 A. Debrassi, A. F. Corrêa, T. Baccarin, N. Nedelko, A. Ślawska-Waniewska, K. Sobczak, P. Dłużewski, J.-M. Greneche and C. A. Rodrigues, *Chem. Eng. J.*, 2012, **183**, 284–293.
55 R. D. Ambashta and M. Sillanpää, *J. Hazard. Mater.*, 2010, **180**, 38–49.
56 S. Chatterjee, D. S. Lee, M. W. Lee and S. H. Woo, *Bioresour. Technol.*, 2009, **100**, 2803–2809.
57 A. M. Etorki and F. M. Massoudi, *Orient. J. Chem.*, 2011, **27**, 875–884.
58 N. Saad, M. Al-Mawla, E. Moubarak, M. Al-Ghoul and H. El-Rassy, *RSC Adv.*, 2015, **5**, 6111–6122.
59 I. Langmuir, *J. Am. Chem. Soc.*, 1918, **40**, 1361–1403.
60 H. Freundlich, *Über die Adsorption in Lösungen*, Engelmann, 1906.
61 O. Redlich and D. L. Peterson, *J. Phys. Chem.*, 1959, **63**, 1024.
62 R. Sips, *J. Chem. Phys.*, 1948, **16**, 490.
63 A. Z. M. Badruddoza, G. S. S. Hazel, K. Hidajat and M. S. Uddin, *Colloids Surf., A*, 2010, **367**, 85–95.
64 R. Sivashankar, A. B. Sathya, K. Vasantharaj and V. Sivasubramanian, *Environmental Nanotechnology, Monitoring & Management*, 2014, **1–2**, 36–49.
65 F.-C. Wu, B.-L. Liu, K.-T. Wu and R.-L. Tseng, *Chem. Eng. J.*, 2010, **162**, 21–27.

66 S. G. Muntean, O. Paska, S. Coseri, G. M. Simu, M. E. Grad and G. Ilia, *J. Appl. Polym. Sci.*, 2013, **127**, 4409–4421.
67 O. M. Paşka, C. Păcurariu and S. G. Muntean, *RSC Adv.*, 2014, **4**, 62621–62630.
68 L. B. L. Lim, N. Priyantha and N. H. M. Mansor, *Environ. Earth Sci.*, 2014, **73**, 3239–3247.
69 T. S. Anirudhan, P. G. Radhakrishnan and K. Vijayan, *Sep. Sci. Technol.*, 2013, **48**, 947–959.
70 E. Bulut, M. Özacar and İ. Şengil, *J. Hazard. Mater.*, 2008, **154**, 613–622.
71 F. Ge, H. Ye, M.-M. Li and B.-X. Zhao, *Chem. Eng. J.*, 2012, **198–199**, 11–17.
72 T. Madrakian and A. Afkhami, *J. Hazard. Mater.*, 2011, **196**, 109–114.
73 K. Singh, S. Gupta, A. Singh and S. Sinha, *J. Hazard. Mater.*, 2011, **186**, 1462–1473.
74 M. Gabal and E. Al-Harthy, *Chem. Eng. J.*, 2014, **255**, 156–164.
75 T. Madrakian, A. Afkhami and M. Ahmadi, *Spectrochim. Acta, Part A*, 2012, **99**, 102–109.
76 L. Ai, C. Zhang and Z. Chen, *J. Hazard. Mater.*, 2011, **192**, 1515–1524.
77 L. Cottet, C. Almeida and N. Naidek, *Appl. Clay Sci.*, 2014, **95**, 25–31.
78 P. Dave, S. Kaur and E. Khosla, *Indian J. Chem. Technol.*, 2011, **18**, 53–60.
79 N. Barka, M. Abdennouri and M. Makhfouk, *J. Taiwan Inst. Chem. Eng.*, 2011, **42**, 320–326.
80 F. Moeinpour, A. Alimoradi and M. Kazemi, *J. Environ. Health Sci. Eng.*, 2014, **12**, 112.
81 O. Elijah and N. T. Joseph, *SOP Transactions on Applied Chemistry*, 2014, **1**, 14–25.
82 J. Pal, M. K. Deb, D. K. Deshmukh and D. Verma, *Appl. Water Sci.*, 2013, **3**, 367–374.
83 E. Bazrafshan, A. Zarei, H. Nadi and M. Zazouli, *Indian J. Chem. Technol.*, 2014, **21**, 105–113.
84 Z. Haddadian and M. Shavandi, *Chem. Sci. Trans.*, 2013, **2**, 900–910.
85 C. Umpuch and S. Sakaew, *Songklanakarin J. Sci. Technol.*, 2013, **35**, 451–459.
86 S. Koner, B. Saha, R. Kumar and A. Adak, *Int. J. Curr. Res.*, 2011, **3**, 128–133.
87 R. Jiang, Y. Fu and H. Zhu, *J. Appl. Polym. Sci.*, 2012, **125**, E540–E549.
88 L. Wang, J. Li, Y. Wang and L. Zhao, *J. Hazard. Mater.*, 2011, **196**, 342–349.
89 S. Lagergren, *About the theory of so-called adsorption of soluble substances, Kungliga Svenska Vetenskapsakademiens, Handlingar 24*, 1898.
90 Y. Ho and G. McKay, *Process Biochem.*, 1999, **34**, 451–465.
91 G. Vijayakumar, R. Tamilarasan and M. Dharmendirakumar, *J. Mater. Environ. Sci.*, 2012, **3**, 157–170.
92 M. Doğan, M. Alkan and Y. Onganer, *Water, Air, Soil Pollut.*, 2000, **120**, 229–248.
93 M. Hema and S. Arivoli, *J. Appl. Sci. Environ. Manage.*, 2008, **12**, 43–51.
94 H. Xu, Y. Xu and Y. Chen, *Adv. Mater. Res.*, 2011, **194–196**, 488–491.
95 M. Arshadi, F. SalimiVahid, J. W. L. Salvacion and M. Soleymanzadeh, *RSC Adv.*, 2014, **4**, 16005.
96 J. X. Zhang and L. L. Ou, *Water Sci. Technol.*, 2013, **67**, 737–744.
97 S. Hong, C. Wen, J. He, F. Gan and Y.-S. Ho, *J. Hazard. Mater.*, 2009, **167**, 630–633.
98 Y. Lin, H. Chen and P. Chien, *J. Hazard. Mater.*, 2011, **185**, 1124–1130.

